LOCA Embrittlement Correlation

M. C. Billone
Argonne National Laboratory
Argonne, IL 60439

April 8, 2005

Executive Summary

The current fixed oxidation limit (17% ECR) has three serious limitations with regard to its application to high burnup fuel and a variety of different cladding alloys. First, it is independent of the amount of hydrogen absorbed in the zirconium-alloy cladding, whereas cladding embrittlement is strongly dependent on hydrogen concentration. Second, it is not sensitive to the actual temperature of the oxidation, such that it does not distinguish between low ductility at 17% ECR accumulated at 1200˚C and ample ductility at 17% ECR accumulated at 1100˚C. Third, it does not give credit for some alloys that might embrittle at a lower ECR, but oxidize at a much slower rate. While it is not possible to replace the fixed oxidation limit with another simple criterion, it is possible to formulate an embrittlement correlation, which is easily calculated with current LOCA analysis methods. The following describes the phenomena, which motivated the formulation of such a correlation, the embrittlement correlation, and the database used to validate the correlation.

Zirconium-alloy cladding has one crystal structure (hexagonal or alpha phase) at reactor operating temperatures and another (body-centered cubic or beta phase) at the higher LOCA-relevant temperatures. The alpha phase has high oxygen solubility and affinity for oxygen, while the beta phase has high hydrogen solubility and affinity for hydrogen. Consequently, during oxidation, some of the beta phase transforms to the high-oxygen-containing alpha phase. Upon cooling, the beta phase remains distinct and is called the prior-beta phase. The surface oxide (mainly ZrO_{2-X}) and the oxygen-rich alpha phase are brittle, so it is only the prior-beta phase (or simply the beta layer) that retains ductility.

In general, the beta layer loses ductility when its average oxygen concentration reaches a critical value ($Co \approx 0.6$ wt.%). However, the beta layer also has a limit on the concentration of oxygen it can hold in solution. This solubility limit So is a function of temperature and hydrogen content such that So can be lower or higher than Co. Figure A illustrates two contrasting situations. The upper set of three diagrams is typical of heavily corroded high-burnup cladding, which has high hydrogen content; this hydrogen in turn produces a high oxygen solubility limit in the beta layer. It is also typical of a high temperature case, for which the oxygen solubility limit is high. As time progresses from t_1 to t_2 to t_3 the average oxygen concentration continues to increase and eventually exceeds the critical concentration at which point the beta layer becomes brittle.

The lower part of Fig. A is typical of fresh cladding that is oxidized at a relatively low temperature (e.g., 1100˚C). In this case, the oxygen solubility limit in the beta layer is quite low. Because the beta layer cannot accommodate oxygen above this limit, additional oxidation causes more and more of the beta layer to transform into alpha. Therefore, as time goes from t_1 to t_2 to

t_3, the oxygen concentration reaches the solubility limit and the beta layer gets thinner and thinner. Although the beta layer remains ductile, the cladding as a whole behaves in a brittle manner because of the vanishing thickness of the beta layer.

To accommodate all of these features, the following embrittlement envelope has been found:

$$Co < 0.6 \text{ wt\%}$$
$$T \leq 1204^{\circ}C \ (2200^{\circ}F)$$
$$ECR \leq 18\%$$
$$\text{Time above } 800^{\circ}C \leq 1 \text{ h}$$

The average oxygen concentration in the beta layer is represented by the following equation:

$$Co = Co(T,t,H) \leq So(T,H)$$

where T is temperature, t is time, H is the initial hydrogen concentration, and So is the beta-phase solubility limit. For time-dependent temperature, Co is calculated by integrating a rate equation. Oxidation is given by the following equation:

$$ECR = E\ Wg(T,t)$$

where E depends on cladding dimensions and Wg is the weight gain, which is calculated using the Cathcart-Pawel (CP) correlation. The CP oxidation correlation is to be used for all alloys at all temperatures. It is a convenient time-temperature correlation, which is a best-estimate weight-gain correlation for Zry-2 and Zry-4; it is not expected to be a best-estimate correlation for all cladding alloys at all relevant steam-oxidation temperatures (e.g., M5 at 1000˚C), but this is not necessary for the empirical approach that has been adopted. An initial set of parameters, consistent with the CP weight gain correlation, has been chosen for the above equations based on post-quench ductility data for fresh Zry-4, ZIRLO and M5, as well as oxygen-content data for prehydrided Zry-4 oxidized at 1200˚C. Post-quench ductility data for prehydrided and high-burnup Zry-4, ZIRLO and M5 will be used to refine these parameters.

The peak cladding temperature (PCT) of 1204°C has been retained for the following reasons. Above ≈1150˚C, ductility in all the alloys begins to decrease rapidly with oxidation and the oxidation rate increases rapidly as temperature increases. Only a very limited amount of time-at-temperature can be tolerated above 1204°C before reaching the critical oxygen concentration and we do not have enough data to describe this difficult regime. It should also be noted that plant thermal-hydraulics calculations become unstable somewhere above 1204˚C (2200˚F), and this was an additional factor in establishing the original cladding temperature limit.

At the other end of the scale, oxidation is very slow at 1000°C and the time (>0.75 h for two-sided oxidation and >2.7 h for one-sided oxidation) required to reach a calculated ECR > 18% is much longer than realistic LOCA times. Also, at these high oxidation times, especially for one-sided oxidation, these alloys experience breakaway oxidation, hydrogen pickup and enhanced embrittlement beyond what is predicted by the embrittlement correlation. Thus, in addition to an ECR limit, a time limit is required for low-temperature oxidation (800-1050˚C).

The parameters in the embrittlement correlation are determined from the post-quench-ductility and oxygen-content data for Zircaloy, ZIRLO and M5. It is believed that the correlation would work for other zirconium-based alloys, but not necessarily all of them. For example, the correlation does not work for the Russian cladding alloy E110 because it develops early breakaway oxidation around 1000°C, resulting in additional hydrogen absorption and enhanced embrittlement at relatively low oxidation times and ECR values.

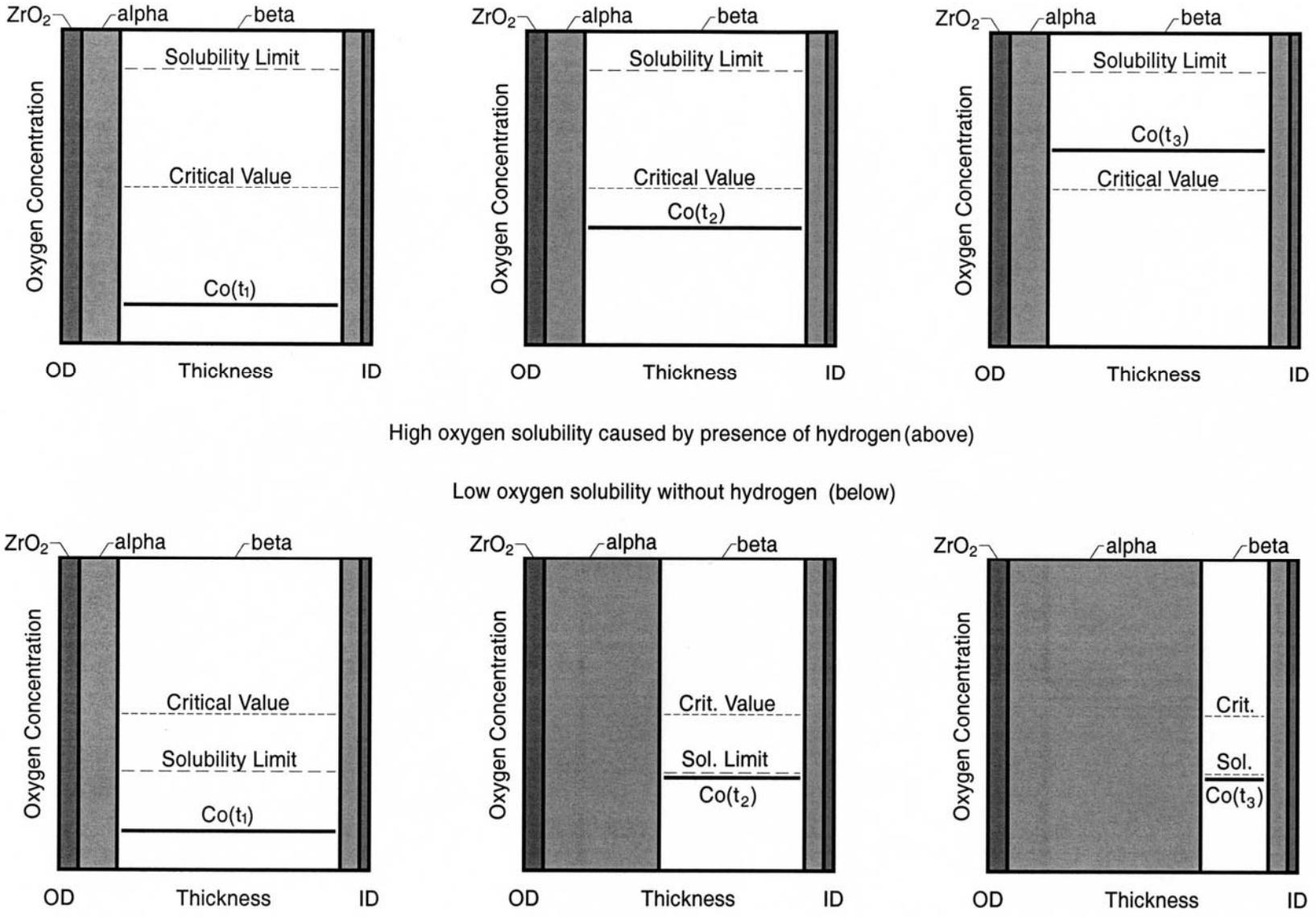

Fig. A. Schematic illustration of embrittlement evolution for cladding with high-hydrogen content (>250 wppm) oxidized at high temperature (above) and for cladding with low-hydrogen content (e.g., fresh cladding) oxidized at low temperature (below).

Technical Summary

ANL post-quench ductility data are summarized for: as-fabricated 17×17 Zry-4, ZIRLO and M5 oxidized to Cathcart-Pawel (CP) calculated ECR values ≤ 20% at 1000˚C, 1100˚C and 1200˚C; prehydrided 17×17 Zry-4 oxidized at 1200˚C to CP-ECR values of 7.5% and 10% and prehydrided 15×15 Zry-4 oxidized at 1200˚C to CP-ECR values of 5% and 7.5%; and high-burnup Zry-4 (800 wppm H) oxidized at ≈1200˚C to a measured ECR value of ≈5.5%. Also presented are post-oxidation ductility results for high-burnup Zry-4 (550 wppm H) oxidized at ≈1200˚C to measured ECR values of ≈5.5% and ≈7.5%. Ductile-to-brittle transition CP-ECR values vs. H-content are determined for Zry-4 oxidized at ≈1200˚C: 5% CP-ECR and ≈600 wppm H, 7.5% CP-ECR and ≈400 wppm H, and 10% CP-ECR and ≈300 wppm H. These transition ECR values are dependent on the oxidation heating rate. The ECR values would be lower for higher heating rates as oxidation at 1200˚C is more embrittling than oxidation at lower temperatures during the ramp to 1200˚C. The high-burnup Zry-4 results are consistent with the prehydrided Zry-4 results when the comparison is made in terms of measured ECR.

ANL and CEA data, as well as other data sets, clearly show three serious limitations in formulating post-quench-ductility criteria in terms of a fixed ECR. First, ECR is independent of hydrogen content, while embrittlement is a very strong function of hydrogen content. Second, ECR integrated over a LOCA or experimental temperature history does not distinguish time spent at high-vs.-low oxidation temperatures, while embrittlement is a strong function of oxidation temperature. Third, some alloys exhibit a low ECR rate (e.g., M5 at 1000˚C) although they embrittle at the same rate as Zry-4, even though their measured or best-estimated ECR value may be low after long times at temperature.

An embrittlement correlation, which accounts for hydrogen content and high-temperature oxidation, is proposed. There are three parts to the proposed correlation: a critical oxygen content (Ccrit in wt.%) in the prior-beta layer at the ductile-to-brittle transition; a beta-layer oxygen solubility limit (So in wt.%), which is a function of temperature and hydrogen content; and a rate equation for determining the time-dependent average oxygen content (Co in wt.%) in the beta layer, which is a function of So, ECR and the weight-gain rate constant K = K(T). For non-irradiated cladding, the rate equation is expressed in terms of CP-ECR and the CP rate constant K. For irradiated cladding the correlation is based on measured ECR. Using Zry-4 data, an initial set of correlation parameters has been chosen. Also, the initial estimate for Ccrit is 0.57 wt.%. A methodology is described for refining correlation parameters and validating the correlation and Ccrit. Following the correlation validation to prehydrided and high-burnup Zry-4 data, prehydrided and high-burnup M5 and ZIRLO data will be used to determine alloy-dependent parameters.

Two additional limits are imposed to prohibit embrittlement at high ECR values due to excessive thinning of the beta layer and to prohibit breakaway oxidation at lower oxidation temperatures: CP-ECR ≤ 18% and time ≤ 1 h at T > 800˚C. The 18% CP-ECR limit is needed to ensure continuity in correlation predictions for 1150-1204˚C and to prevent excessive thinning of the beta layer for 1050-1150˚C. The time limit is needed to prevent breakaway oxidation and enhanced embrittlement for 800-1050˚C. Also, as the data base is limited to ≤1204˚C-oxidation temperatures, and the embrittlement rate is very high for >1204˚C, 1204˚C is retained as the PCT.

1. Introduction

The LOCA criteria in 10 CFR 50.46 (PCT ≤ 2200˚F [1204˚C], ECR ≤ 17%) are intended to ensure that cladding maintains some ductility during and following quench. The 1204˚C temperature limit (PCT) and 17%-ECR oxidation limit, expressed as equivalent cladding reacted (ECR), are based on Hobson's [1] ring-compression test data for non-irradiated Zry-4 cladding samples containing low hydrogen concentration (≈10 wppm). The ECR values for Hobson's samples were determined using the Baker-Just (BJ) correlation. At 1204˚C, 17% BJ-ECR corresponds to a best-estimate Cathcart-Pawel (CP) ECR of 13%. In 1980, Chung and Kassner [2] proposed an alternative set of criteria based on thermal shock tests and energy-limited (0.3-J) impact tests of oxidized Zry-4 cladding. Their criteria for surviving thermal shock during quench and post-quench impact loads without fragmentation are: calculated oxygen content in the prior-beta layer ≤ 0.7 wt.% and measured prior-beta-layer thickness > 0.3 mm.

The experimental work at ANL has been designed to quantify the post-quench ductility of Zry-2, Zry-4, ZIRLO and M5 cladding alloys in the as-fabricated condition and after high-burnup operation. Studies of post-quench ductility of non-irradiated, prehydrided Zry-4 have also been conducted to help plan the high-burnup Zry-4 experiments and to add to our understanding of hydrogen-enhanced embrittlement following high-temperature steam oxidation.

Based on the ANL results, it is clear that post-quench ductility and ductile-to-brittle transition ECR are highly dependent on hydrogen content and oxidation temperature history. The temperature history is very important because oxidation (ECR) during the heating, as well as the cooling, ramp, is less embrittling than oxidation at the hold temperature, particularly at ≈1200˚C. In the ANL program, post-quench ductility is being determined at 135˚C to be consistent with the temperature at which the original regulation was based. Testing at other temperatures (e.g., room-temperature [RT] and 100˚C) has been performed and may be done again in the future. The 135˚C temperature is sufficient to demonstrate that ductility is preserved during and immediately following the ECCS quench.

Experimental results generated at ANL, CEA and other laboratories have demonstrated that as-fabricated cladding alloys (Zry-4, ZIRLO, and M5) oxidized at 1000-1100˚C retain post-quench ductility at RT for calculated ECR values ≥ 20% corresponding to test times ≤ 1h (see Figs 1-4 for ANL RT data); and that these as-fabricated cladding alloys oxidized at 1200˚C retain post-quench ductility at 135˚C for calculated ECR values ≥ 17% (see Figs 5-7 for ANL RT and 135˚C data). Extrapolation of the data in Figs. 5-7 suggests that these alloys oxidized at 1200˚C lose ductility at ≈18% CP-ECR. However, as shown in Fig. 8 (ANL data for 17×17 Zry-4) and Fig. 9 (ANL data for 15×15 Zry-4) prehydrided (≥300 wppm) Zry-4 oxidized at 1200˚C exhibits post-quench embrittlement at 135˚C at ≤ 10% CP-ECR. Specifically, the ductile-to-brittle transition for 1200˚C-oxidized Zry-4 occurs at hydrogen contents and CP-ECR values of: 600 wppm and 5%; 400 wppm and 7.5%; and 300 wppm and 10%. These particular transition ECR values are dependent on temperature history – mainly the temperature ramp during heating. However, the test results clearly show the embrittling effects of hydrogen during steam oxidation.

ANL results show that ECR values (CP-ECR) calculated with the Cathcart-Pawel weight gain correlation [3] are in good agreement with the ANL-measured ECR values for all as-fabricated

and prehydrided alloys oxidized at 1200˚C, although deviation at lower temperatures is observed for some alloys (e.g., M5 at 1000˚C). For practical reasons, it is often convenient to refer to the calculated ECR values, especially for non-irradiated cladding. For high-burnup cladding, it is more representative to use the measured transient ECR values, as the corrosion layer is partially protective: it slows down early time oxidation rate relative to the predictions and data for bare, non-irradiated cladding. More data are needed to develop a best-estimate model or correlation for oxygen embrittlement vs. ECR and hydrogen for corroded, irradiated cladding.

The fundamental problem of trying to correlate post-quench ductile-to-brittle transition to ECR or weight gain is that most of the weight gain is associated with the formation of a brittle oxide layer, some of the weight gain is associated with the formation of a brittle oxygen-stabilized alpha layer, and only a small fraction of the weight gain is associated with oxygen pickup in the beta layer. Yet, embrittlement is a strong function of this oxygen concentration in the beta layer, which in turn is a strong function of oxidation time, temperature and hydrogen content. ECR, on the other hand, is independent of hydrogen content. While ECR continues to increase with time-at-temperature, the oxygen content in the beta layer – prior-beta layer after cooling – saturates at the solubility limit. This solubility limit for oxygen concentration in the beta layer is alloy dependent. For each alloy, it is a function of temperature and hydrogen concentration in the beta layer. The solubility limit also has a significant effect on the rate of increase of beta-layer oxygen concentration during isothermal oxidation tests, as well as during time-dependent temperature histories.

In the current work, the post-quench ductile-to-brittle transition is assumed to occur at a critical average oxygen concentration (Ccrit) in the prior-beta layer. A rate correlation is proposed for calculating the increase in beta-layer oxygen concentration with time for transient temperature histories. The rate correlation is essential for analysis of the ANL data, for analysis of other post-quench-ductility data sets, and for performing in-reactor calculations for transient LOCA temperature histories. Parameters in the rate equation, as well as the critical oxygen concentration value, are determined from post-quench ductility data. Although the oxygen concentration in the beta layer is very difficult to measure, weight gain and corresponding ECR, post-quench ductility and microhardness are relatively easy to measure. The rate correlation proposed in this current effort expresses the average oxygen concentration in the beta layer as a function of temperature, hydrogen content, and ECR. There is a practical consideration in expressing the oxygen concentration in terms of ECR as LOCA codes currently include algorithms for calculating ECR as a function of time for time-dependent temperature histories.

The approach adopted in the current work is to determine the embrittlement-correlation parameters to be consistent with the database for prehydrided and high-burnup Zry-4. Based on ANL post-quench-ductility data, the Zry-4 parameters should give a lower-bound ductile-to-brittle transition for ZIRLO and M5 in the as-fabricated condition. Following the determination of a set of parameters for Zry-4 and embrittlement-correlation validation, the correlation will be tested against the data for prehydrided and high-burnup ZIRLO and M5 to determine alloy-dependent effects on the parameters and the critical oxygen concentration.

Based on a preliminary analysis of ANL Zry-4 data, the critical oxygen content for Zry-4 appears to be in the range of 0.5-0.7 wt.%. It is interesting to note that Chung and Kassner established an oxygen concentration limit of 0.7 wt.% based on energy-limited (0.3 J) impact tests conducted at room temperature. The 0.7 wt.% is the calculated oxygen concentration at the mid-wall for two-sided oxidation or the beta-layer oxygen concentration at the inner surface for one-sided (outer-surface) oxidation. As the ANL database used to determine correlation parameters is limited to ≤ 20% CP-ECR test conditions, which corresponds to a predicted minimum beta-layer thickness of ≈0.36 mm for 17×17 Zry-4 (0.57-mm wall thickness), a CP-ECR limit is also imposed to protect against embrittlement due to excessive thinning of the beta layer. Some limit on ECR or prior-beta layer thickness is needed because shrinkage of this layer with increasing ECR will eventually cause brittle failure of a compressed ring regardless of the beta-layer oxygen content and local ductility. As weight gain and corresponding ECR are more accurately predicted by the CP correlations than the beta-layer thickness for ECR > 13%, the limit to preclude excessive thinning of the beta layer is based on predicted ECR rather than on predicted beta-layer thickness.

Chung and Kassner restricted the measured beta layer to be >0.3 mm, along with the 0.7 wt.% oxygen-concentration limit, for survival of 0.3-J impact. Although the proposed criteria are similar to the Chung and Kassner criteria in that limits are placed on both the beta-layer oxygen concentration and beta-layer thickness, it is likely that the critical oxygen concentration to ensure post-quench ductility will be lower than the critical oxygen concentration to ensure survival of the 0.3-J impact. Impact resistance is a combination of strength and ductility, but even a brittle material may have enough strength to survive a limited-energy impact without failure.

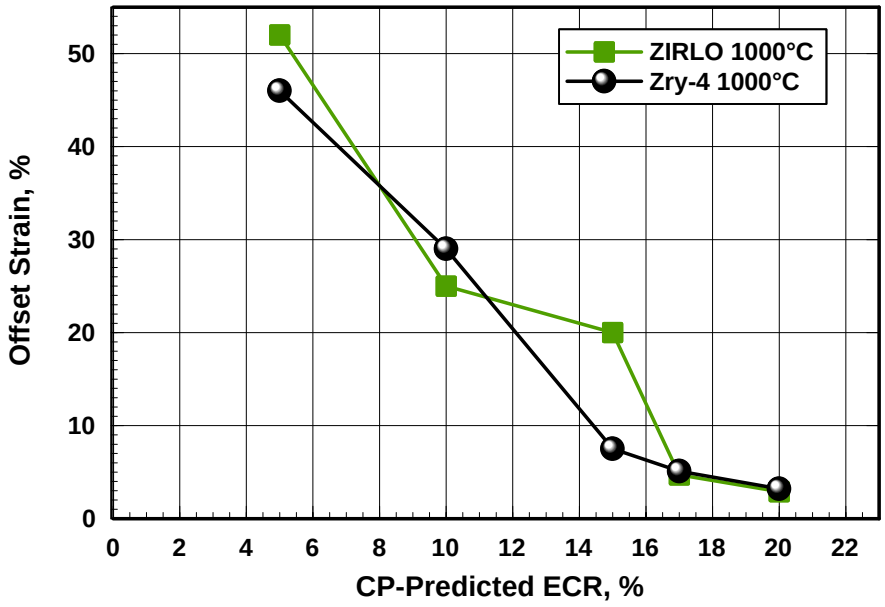

Fig. 1. Post-quench ductility vs. CP-predicted ECR for ZIRLO and Zry-4 oxidized in steam at 1000˚C. Ductility is based on offset strain (≥2%) determined from ring-compression tests conducted at room temperature and 2 mm/min. cross-head displacement rate.

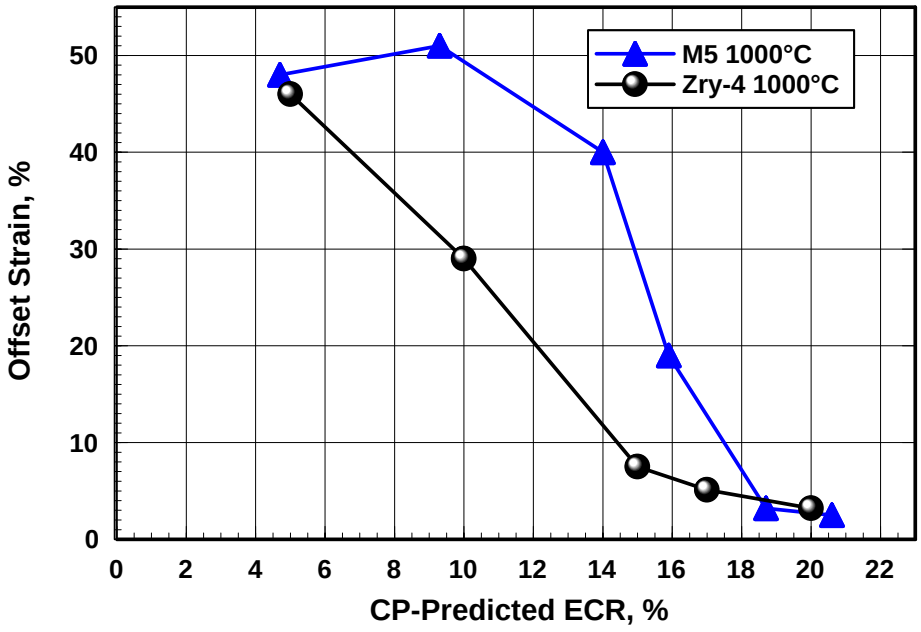

Fig. 2. Post-quench ductility vs. CP-predicted ECR for M5 and Zry-4 oxidized in steam at 1000˚C. Ductility is based on offset strain (≥2%) determined from ring-compression tests conducted at room temperature and 2 mm/min. cross-head displacement rate.

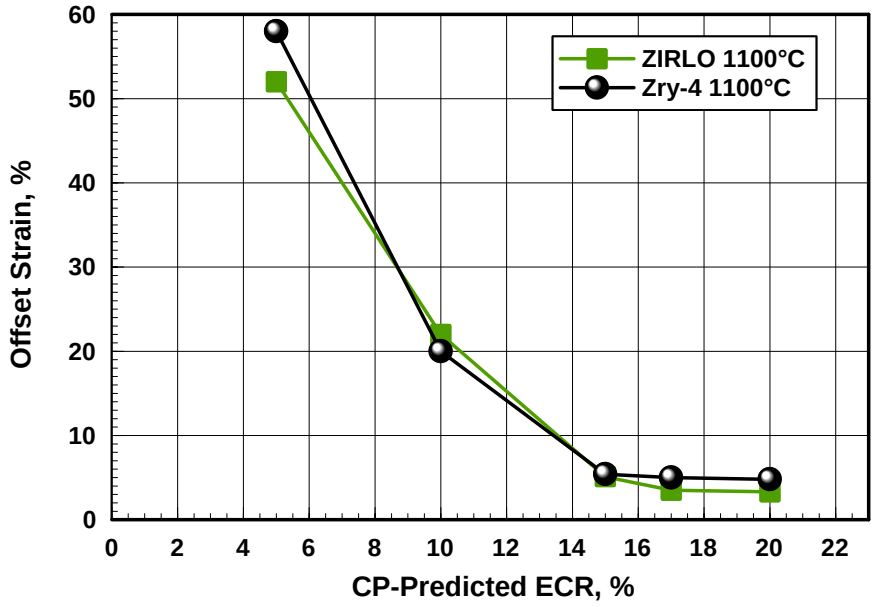

Fig. 3. Post-quench ductility vs. CP-predicted ECR for ZIRLO and Zry-4 oxidized in steam at 1100˚C. Ductility is based on offset strain (≥2%) determined from ring-compression tests conducted at room temperature and 2 mm/min. cross-head displacement rate.

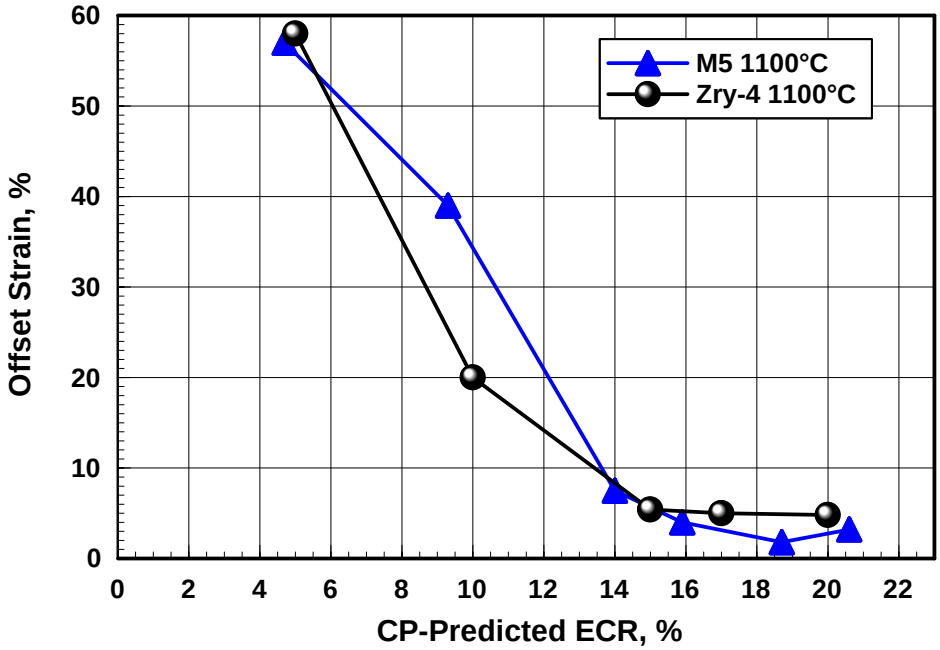

Fig. 4. Post-quench ductility vs. CP-predicted ECR for M5 and Zry-4 oxidized in steam at 1100˚C. Ductility is based on offset strain (≥2%) determined from ring-compression tests conducted at room temperature and 2 mm/min. cross-head displacement rate.

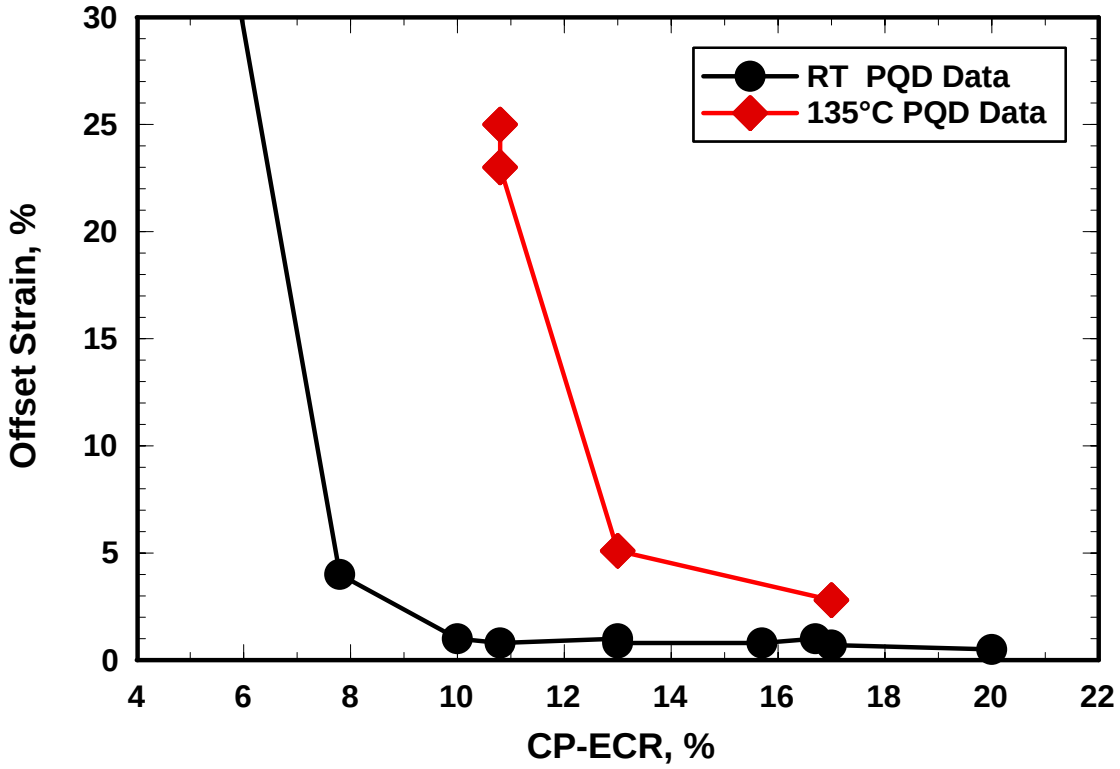

Fig. 5. Offset strain vs. CP-predicted ECR for 17×17 Zry-4 (9.50-mm OD, 0.57-mm wall thickness) oxidized at 1200˚C, slow-cooled to 800˚C and quenched. The results are from ring-compression tests conducted on ≈8-mm-long samples at a displacement rate of 0.0333 mm/s (0.35%/s) and at both room temperature and 135˚C.

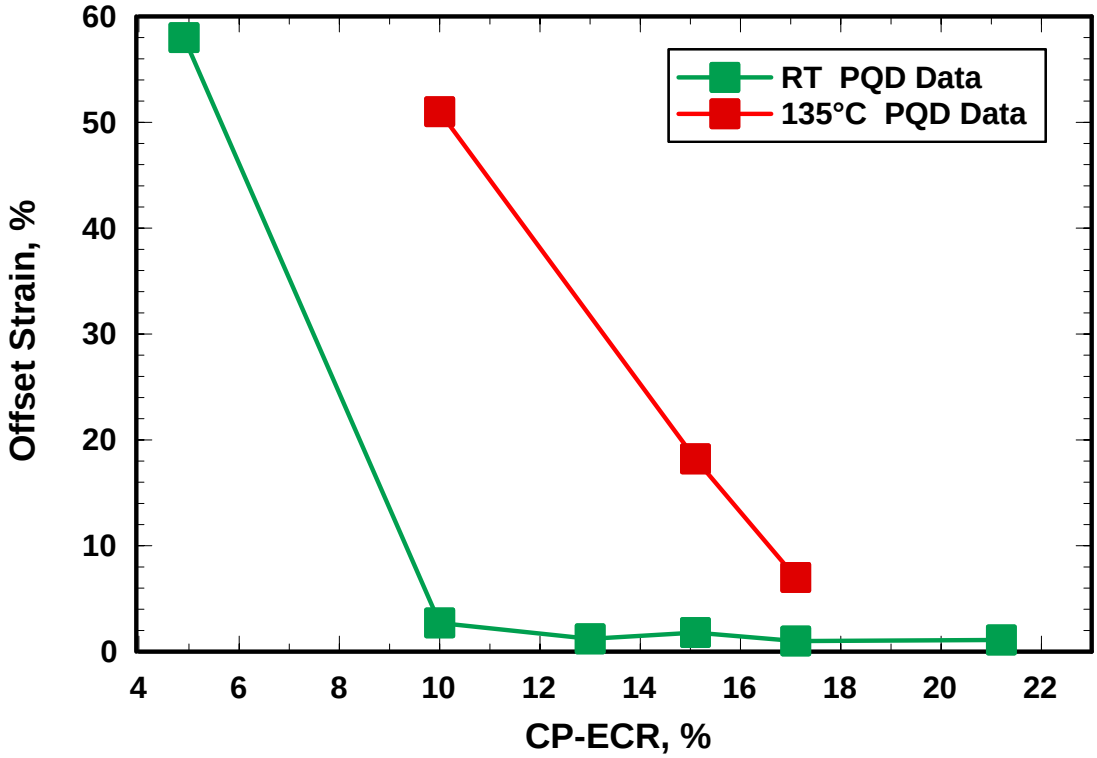

Fig. 6. Offset strain vs. CP-predicted ECR for 17×17 ZIRLO (9.50-mm OD, 0.57-mm wall thickness) oxidized at 1200˚C, slow-cooled to 800˚C and quenched. The results are from ring-compression tests conducted on ≈8-mm-long rings at room temperature (RT) and a displacement rate of 0.0333 mm/s (0.35%/s) and on ≈5-mm-long samples at 135˚C and 0.35%/s.

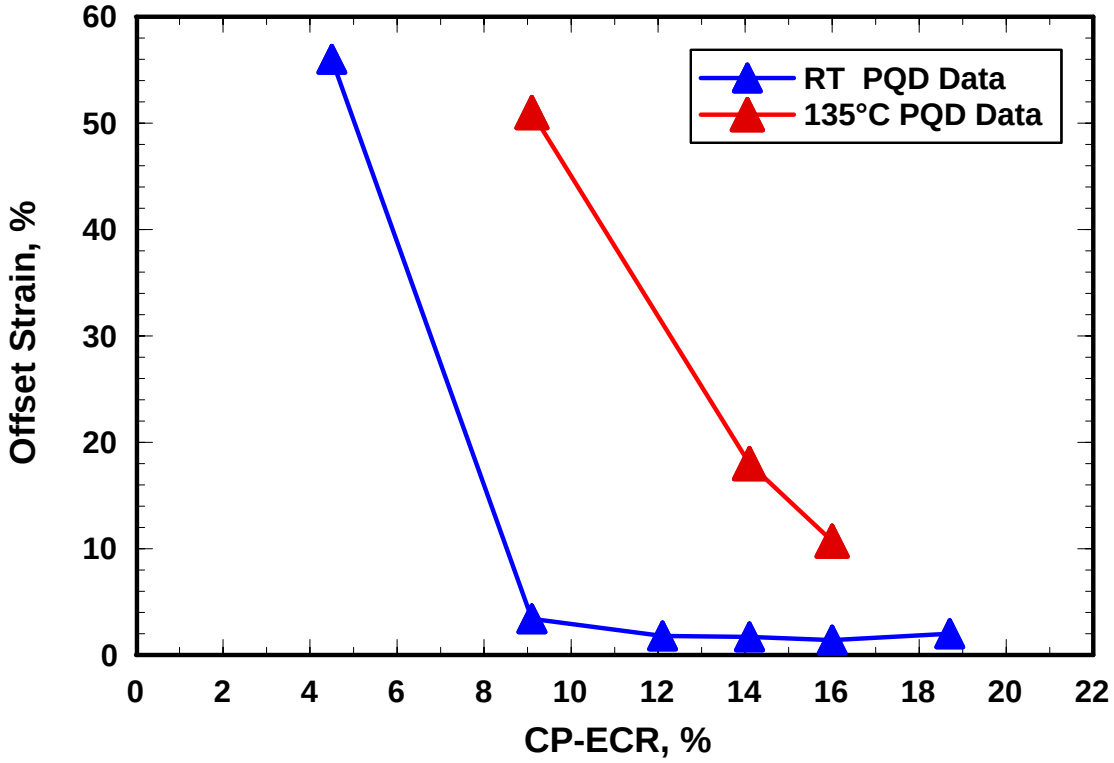

Fig. 7. Offset strain vs. CP-predicted ECR for 17×17 M5 (9.50-mm OD, 0.61-mm wall thickness) oxidized at 1200˚C, slow-cooled to 800˚C and quenched. The results are from ring-compression tests conducted at room temperature (RT) and 135˚C on ≈8-mm-long samples at a displacement rate of 0.0333 mm/s (0.35%/s).

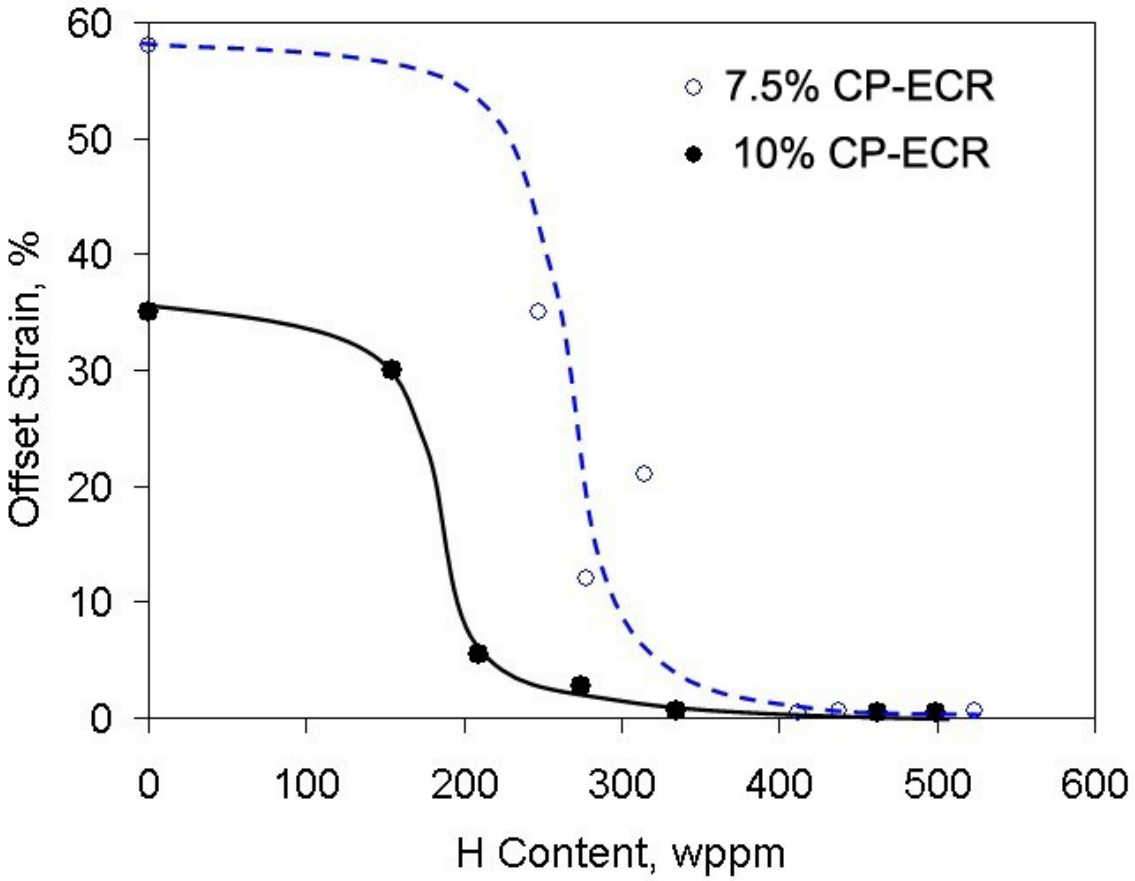

Fig. 8. Post-quench ductility at 135˚C of as-received and prehydrided 17×17 Zry-4 oxidized at 1200˚C to two ECR values, cooled at ≈10˚C/s to 800˚C and quenched at 800˚C. CP-predicted ECR values are 7.5% and 10%, while measured values are closer to 8.5% and 10.5%.

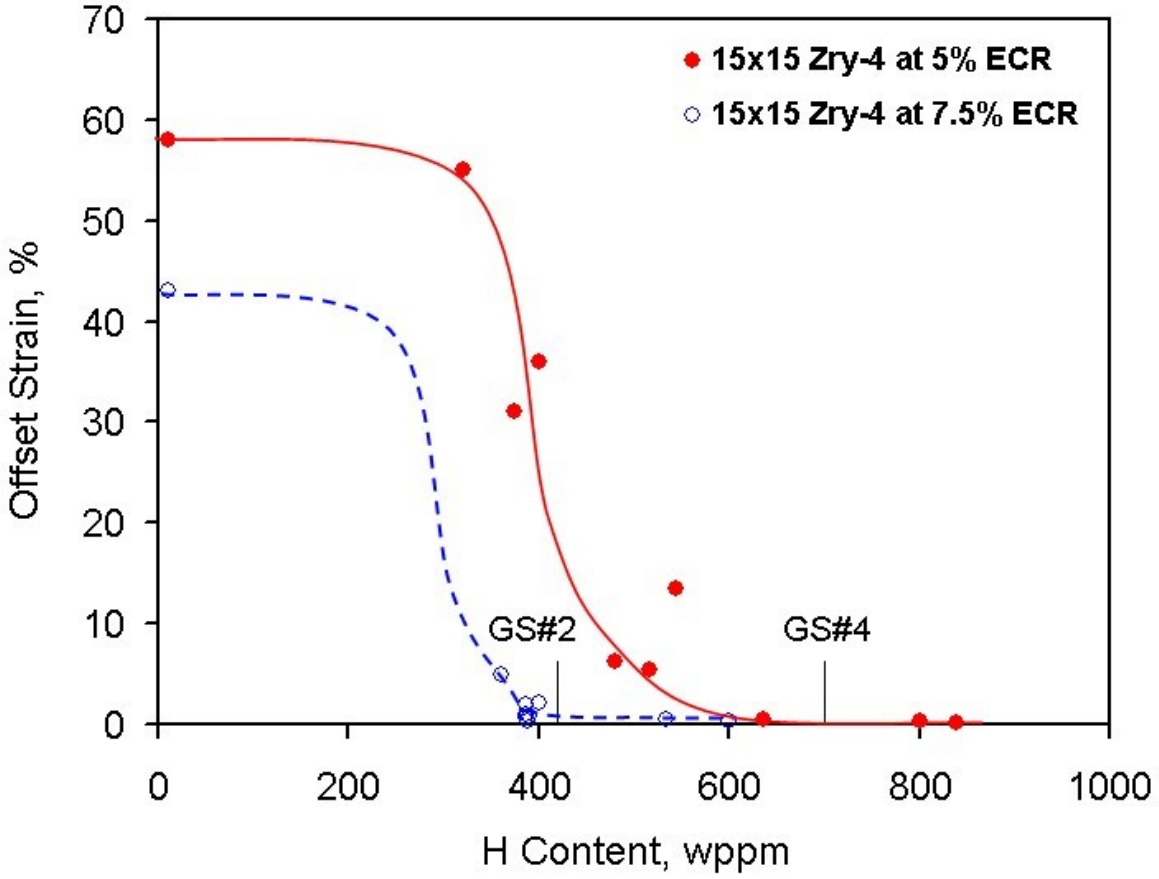

Fig. 9. Post-quench ductility at 135˚C of as-received and prehydrided 15×15 Zry-4 oxidized at 1200˚C to two CP-predicted ECR values, cooled at ≈10˚C/s to 800˚C and quenched at 800˚C. GS#2 and GS#4 refer to the mid-points of grid spans 2 and 4 of the H.B. Robinson (HBR) high-burnup Zry-4, which is being used to section LOCA integral test samples. Short samples (25-mm long) from near the bottom of grid span 4 (550±90 wppm) have already been exposed to two-sided oxidation at 1204˚C and ring-compression testing at 135˚C. One-sided oxidation tests are being conducted under the same conditions for 38-mm-long samples from a sibling HBR rod.

2. Weight Gain and ECR

Weight gain (Wg) is both measurable and easily calculated based on correlation and model predictions (e.g., Cathcart-Pawel correlation and models). The relationship between ECR (in %) and weight gain (in mg/cm^2) is:

Outer-surface oxidation (1-sided): $ECR = (0.4385\ Wg/h)/(1 - h/Do)$ (1a)

Double-sided oxidation (2 sided): $ECR = (0.8769\ Wg/h)$ (1b)

where h = cladding wall thickness in mm and Do = cladding outer diameter in mm. For 17×17 PWR cladding with 9.50-mm outer diameter and 0.57-mm wall thickness, ECR = 0.818 Wg for outer-surface oxidation and ECR = 1.538 Wg for double-sided oxidation.

Evaluating ECR vs. time during a LOCA transient requires that the weight-gain rate equation be integrated with respect to temperature (with time implicit) or with respect to time. The rate equation form is based on parabolic kinetics. Integration of this rate equation gives:

$$(Wg)^2 - (Wgi)^2 = \int_0^t K^2\, dt \quad (2a)$$

where the commonly used Cathcart-Pawel (CP) correlation for the rate constant, K vs. T (in Kelvin), based on stoichiometric oxide (ZrO_2), is given by

$$K = 601.83 \exp(-10{,}050.33/T)\ mg/(cm^2\ s^{0.5}) \quad (2b)$$

and the more accurate, but less frequently used CP-correlation for K, based on hypostoichiometric oxide (ZrO_{2-X}), is given by

$$K = 579.66 \exp(-10{,}032.71/T)\ mg/(cm^2\ s^{0.5}) \quad (2c)$$

As can be seen by substituting the rate constant K = K(T) from Eq. 2b into Eq. 2a, the integration over the T = T(t) LOCA history or experimental temperature history must be done numerically because no analytical solution exists for this integration.

3. Solubility of Oxygen in the Beta Phase for T ≥ 1000˚C (1273K)

Chung and Kassner [4] give the following correlation for the solubility (So in wt.%) of oxygen in the beta phase for as-fabricated Zry-4 (i.e., low hydrogen content):

$$So = \exp(5.02 - 8220/T) \quad (3)$$

Equation 3 predicts 0.24 wt.% at 1000˚C, 0.38 wt.% at 1100˚C, 0.57 wt.% at 1200˚C, 0.58 wt.% at 1204˚C and 0.7 wt.% at 1256˚C. ANL data show that as-fabricated 17×17 low-tin Zry-4 and ZIRLO oxidized at 1200˚C retain post-quench ductility at 135˚C up to ECR values >17% (>16% for M5), by which time ≈93% saturation of the beta layer is predicted to occur. To the extent that Eq. 3 is accurate, then the ductile-to-brittle oxygen concentration in the beta layer should be

> 0.53 wt.%. The results have been confirmed for modern 15×15 M5 and will be confirmed for modern 15×15 low-tin Zry-4. However, post-quench ductility for older (1975-1990), standard 15×15 Zry-4 show that 135˚C-test post-quench ductility is lost at 13% CP-ECR (14% measured ECR). Other than having higher as-fabricated oxygen content (0.14 wt.% vs. 0.12 wt.%), it is not clear why the rougher, older cladding does not perform as well as the smooth-surface modern cladding. The embrittlement correlation developed in this work is based on modern-cladding data and might not bound the case for older as-fabricated cladding, which embrittles at a calculated beta-phase oxygen content of ≈0.5 wt.% and ≈13% CP-ECR for 1204˚C oxidation temperature. However, consistent with current criteria, the older cladding does maintain ductility for T ≤ 1204˚C and BJ-ECR ≤ 17%.

The CEA studies (ASTM-2004 [5] and NRC-2004 [6]) indicate that the oxygen solubility limit in the beta phase of Zry-4 may be higher than 0.57 wt.%. CEA measured 0.72-wt.% oxygen in as-fabricated Zry-4 after 520 s of outer-surface oxidation at 1200˚C. They also measured 0.92-wt.% oxygen in 320-wppm prehydrided Zry-4 after 605 s at 1200˚C (13% CP-ECR) and 1.1±0.1 wt.% oxygen in both 620-wppm Zry-4 after 1470 s (20.5% CP-ECR) and 730-wppm Zry-4 after 1505 s (20.8% CP-ECR) at 1200˚C. The results strongly support oxygen-solubility enhancement with increasing hydrogen content, as well as saturation of this effect at ≤600 wppm H. Although more data would be needed to derive the dependence of solubility on temperature and hydrogen content, a simplified correlation is assumed for the current work:

$$So = \exp (5.02 - 8220/T) + \Delta S \, (1 - \exp [-aC_h]) \qquad (4)$$

where $\Delta S = \Delta S \, (T, C_h)$, $a = a \, (T)$, and C_h = hydrogen concentration in wppm. Based on the CEA results at 1200˚C oxidation temperature, values for ΔS and "a" can be estimated to be ≈0.6 wppm and $\approx 6.0 \times 10^{-3}$ at this oxidation temperature. The $\Delta S(T, C_h)$ and a(T) functions could be determined from extension of the CEA work to other oxidation temperatures and hydrogen contents. These functions could also be derived indirectly based on post-quench ductility data for prehydrided Zry-4 oxidized at 1000˚C and 1100˚C. As such data are not currently available, the following trial function is recommended for 1000-1200˚C oxidation temperatures:

$$So = \exp (5.02 - 8220/T) + 0.6 \, (1 - \exp [-6 \times 10^{-3} \, C_h]) \qquad (4a)$$

Equation 4a is intended for initial validation of the embrittlement correlation. It matches the CEA data for 620-wppm and 730-wppm Zry-4 oxidized at 1200˚C to ≈20% ECR. For the 320-wppm H, it predicts a solubility limit of 1.08 wppm > 0.92 wppm measured. The beta layer in this sample has not reached its solubility limit after 605 s (13% ECR) of oxidation at 1200˚C.

4. Rate Equation for Average Oxygen Content in the Beta Layer

4.1 Fundamental approach

Let Coi be the as-fabricated oxygen content in the cladding (≈0.12-0.14 wt.%) and let Co (≤So) be the average oxygen concentration in the beta layer during the LOCA thermal history. The fundamental approach would involve solving the oxygen diffusion equation in the beta layer and including the moving alpha-beta interface layer, which decreases the thickness of the beta layer

as a function of time at temperature. This approach leads to a very complicated set of equations. The equations are too complicated for a single rate correlation even if the moving boundary is ignored and the cladding wall is treated as a flat plate. In this approach, the boundary conditions for the oxygen concentration $c_o = c_o(y,t)$ in the beta layer at the alpha-beta boundary would be the solubility limit So. The boundary condition at the other surface for one-sided oxidation would be no oxygen concentration flux at this boundary ($\partial c_o/\partial y = 0$); for two-sided oxidation, the no-flux condition would be imposed at the plate mid-thickness. The solution to the fixed-boundary problem can be found in both conductive heat transfer and diffusion theory textbooks. The full analytical solution involves an infinite series of the products of cosines of position and exponentials of time. Short-time, intermediate-time and long-time approximations can be derived, but no simple analytical solution is available to cover the full time interval for Coi → So. Figure 10 shows the heat-transfer equivalent solution to this problem. Translating this figure into diffusion terminology, T_0 is the initial oxygen concentration (Coi), T_1 is the oxygen solubility limit (So), b = thickness of beta layer, y = b is the alpha-beta boundary, and α is the diffusivity (D) of oxygen in the beta phase. As can be seen from Fig. 10, the parameter $\tau = b^2/\alpha = b^2/D$ is often referred to as the characteristic time to reach equilibrium (≈ Coi + 0.93[So – Coi] for this problem).

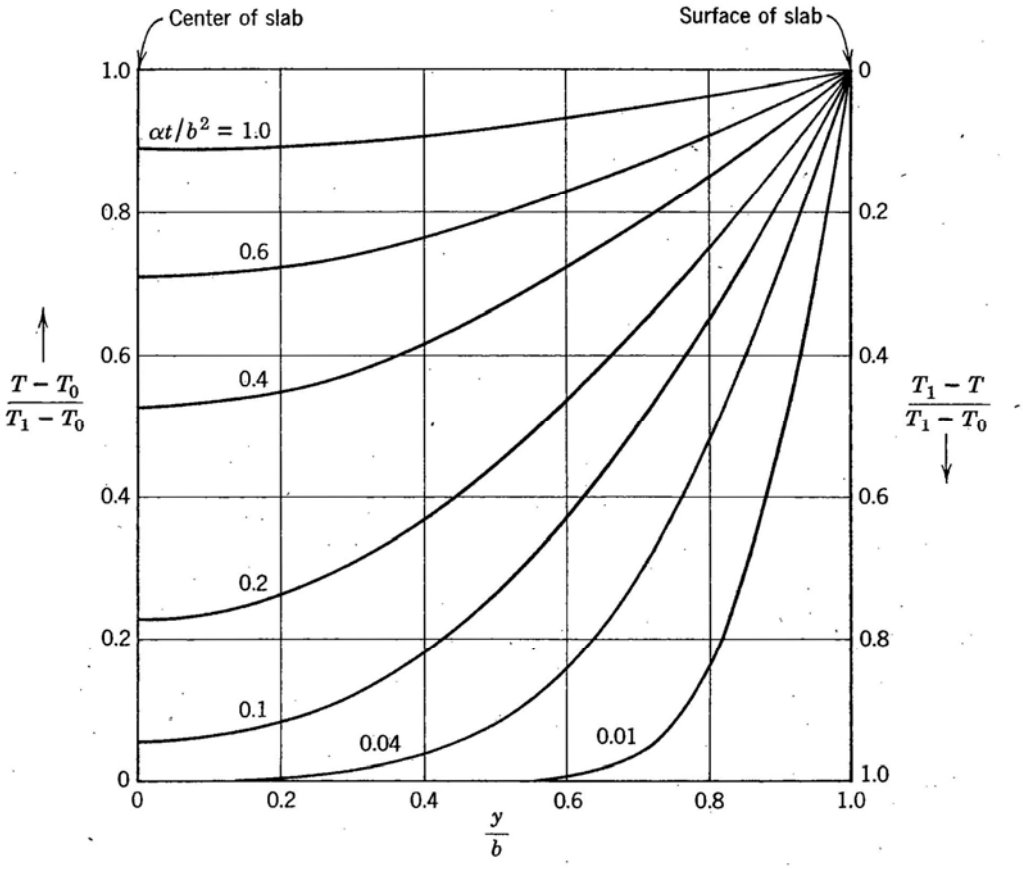

Fig. 10. Temperature profiles for unsteady-state heat conduction in a slab of finite thickness. [H. S. Carslaw and J. C. Jaeger, *Conduction of Heat in Solids*, Oxford University Press (1959), p. 101].

For the problem solved graphically in Fig. 10, a solution is also available for the average temperature vs. time. This is shown graphically (see Curve I) in Fig. 11 from Carslaw and Jaeger. Translating to the diffusion problem, let D = κ, (Co-Coi)/(So-Coi) = v/V and let b = *l* = beta layer thickness.

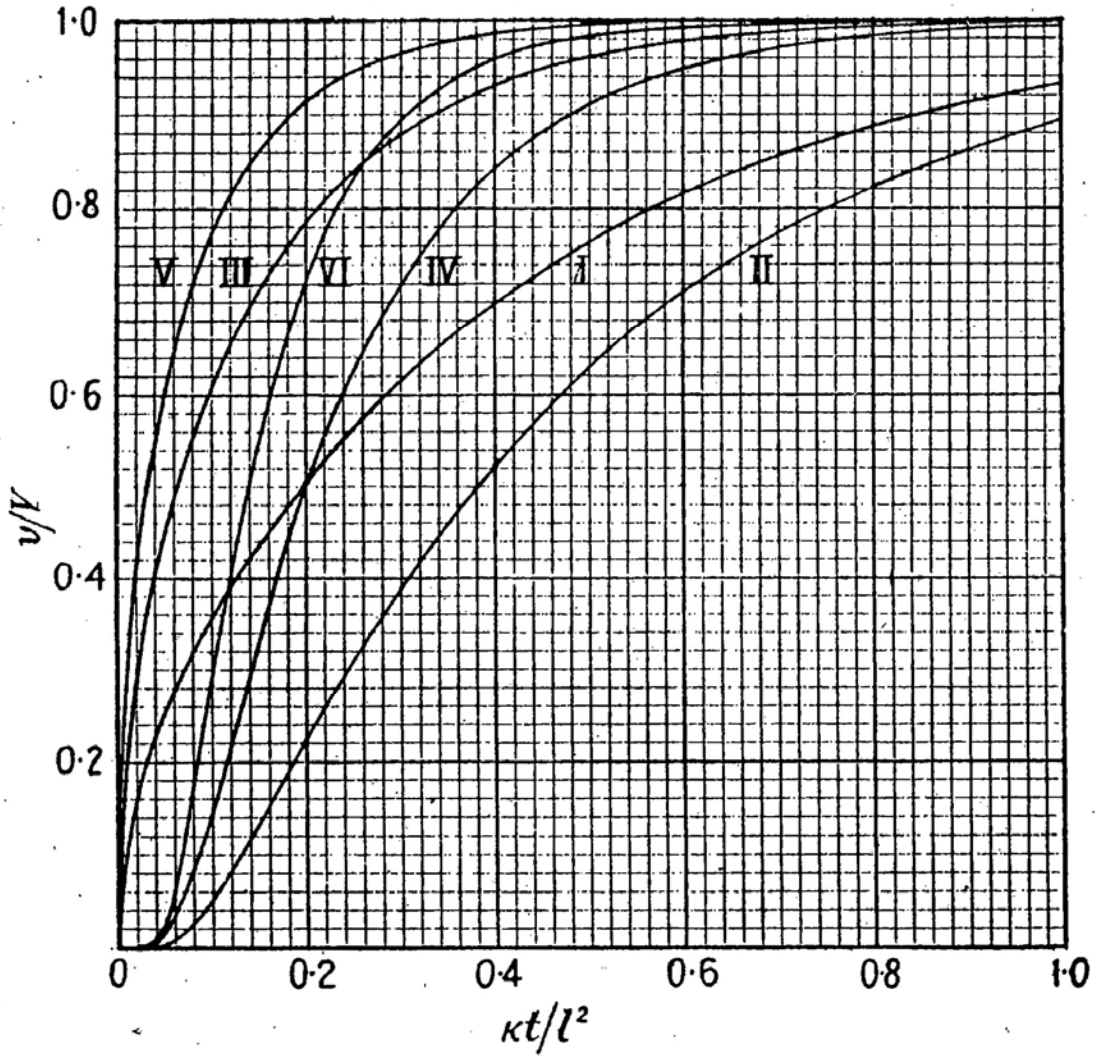

Fig. 11. Center and average temperatures for a slab of thickness 2*l* (curves II and I); for an infinite cylinder of diameter 2*l* (IV,III); and for a sphere of diameter 2*l* (VI,V). Initial temperature zero and surface temperature *V*. [H. S. Carslaw and J. C. Jaeger, *Conduction of Heat in Solids*, Oxford University Press (1959), p. 102].

The diffusion solution is:

$$(Co - Coi)/(So - Coi) = 1 - (8/\pi^2) \Sigma (2n + 1)^{-2} \exp [-D (2n + 1)^2 \pi^2 t/(4b^2)] \quad (5)$$

and

$$Co = Coi + (So - Coi) \{1 - (8/\pi^2) \Sigma (2n + 1)^{-2} \exp [-D (2n + 1)^2 \pi^2 t/(4b^2)]\} \quad (5a)$$

As can be seen from the Carslaw-Jaeger Fig. 11, the increase in the average concentration slows down considerable for the normalized time $(Dt/b^2) > \approx 0.7$. However, for the cladding problem, the thickness "b" is decreasing with time and the rate of increase of Co with time is faster than shown in the figure.

The diffusion coefficient given by Perkins et al. [7] for oxygen in the beta phase of Zry-4 is:

$$D = 0.0263 \exp (-28200/RT) \text{ cm}^2/\text{s} = 1.72 \times 10^{-6} \text{ cm}^2/\text{s at } 1200^\circ\text{C} \quad (6)$$

For oxidation of 17×17 Zry-4 (9.50-mm OD, 0.57-mm thickness), ANL data give a beta-layer thickness of 0.0419 cm at 13% ECR and 0.0266 cm at 20% ECR. For one-sided oxidation at 1200˚C, 13% ECR corresponds to ≈590 s and $(tD/b^2) = t/\tau \approx 0.6$. Thus, at 13% ECR and 1200˚C, the beta layer would have ≤ 0.12 + 0.82 (0.57 - 0.12) wt.% = 0.49 wt.%, which is ≈86% saturation of So. Although the times would be lower for two-sided oxidation, the percent saturation vs. ECR would be about the same. This calculation is very approximate as it uses the final value of the beta-layer thickness at 13% ECR, rather than the time-dependent values.

Computer modeling codes have been developed to treat oxygen diffusion through the oxide layer, the alpha layer and the beta layer, as well as the growth of the oxide and alpha layers (moving boundary problem). This approach is appealing because the existence of hydrogen in the beta layer would increase average oxygen concentration vs. time in two ways: by increasing the short-time diffusion rate during which oxygen increases in the beta layer due to the higher initial concentration gradient (So – Coi) and by increasing the long-time oxygen concentration due to the higher value of the saturation limit So. However, for the purposes of the current work, it is recommended that such codes be used to benchmark and validate the empirical rate correlation developed in the next section. Also, the models in these codes have generally been benchmarked to data from short-time isothermal tests at relatively low ECR values. Although they can be used to predict weight gain and oxide layer thickness reasonably well up to 20% ECR, it is not clear how well they predict the oxygen profile and average oxygen content in the beta layer, as well as the beta layer thickness, for higher ECR values. ANL experience with such modeling suggests that the alpha-layer thickness is under-predicted and the beta-layer thickness is over-predicted by such models for ECR > 13%.

4.2 Empirical Approach

The fundamental approach described in 4.1 makes the assumption that the rate limiting step in oxygen increase in the beta layer is diffusion of oxygen across the beta layer with fixed boundary condition $c_o(b,t) = So$ at the oxidizing surface of the beta layer. If the rate limiting step were diffusion of oxygen through the oxide and alpha layers, then it would be more appropriate to use weight gain or ECR as the fundamental parameter for determining Co. Even if this were not the case throughout the whole temperature history, it is an appealing approach because ECR is already calculated in current LOCA codes. The relationship between Co and ECR can be approximated by correlating the two variables based on modeling code predictions. ANL has performed preliminary code calculations to compare Co(t) to ECR(t) for thicker 15×15 cladding (0.76 mm) and thinner 17×17 (0.57 mm) cladding, both oxidized at 1200˚C. The results show excellent correlation between ECR and average oxygen concentration in the beta layer, independent of cladding thickness. Figure 12 shows the predicted increase in average oxygen content of the beta layer with ECR. The ANL computer model has been constructed to give reasonably good predictions for weight gain, given measured oxide-, alpha- and beta-layer thicknesses. It also has the Cathcart-Pawel models for predicting these thicknesses. However, rather than solving the problem for simultaneous diffusion and moving boundaries, the code calculates the layer thicknesses for a particular temperature history. A diffusion calculation is then performed for this final geometry to determine oxygen-concentration profiles across each layer, as well as average oxygen content. Also, the zero-flux boundary condition for the beta layer is not modeled precisely. Rather, the fixed-concentration condition, co = Coi, is imposed at an infinite distance away from the alpha-beta boundary. Thus, Fig. 12 should be used to demonstrate the trend for average beta-layer oxygen concentration vs. ECR, rather than for precise values.

For development of an empirical correlation, what is needed is a simple integrable function of Co vs. ECR that saturates at the solubility limit as ECR increases. Following the approach for the solutions shown in the Carslaw-Jaeger Figs. 10 and 11, two simple functions were considered to match the variation of the normalized function (Co - Coi)/(So – Coi) with ECR: a simple exponential function, [(1 - exp(-A·ECR)], which increases from 0 to 1 with monotonically decreasing slope as Co → So, and a bi-linear function, which increases from 0 to 1 at a particular ECR and is fixed at 1 for higher ECR values. The exponential function did not give a very good fit to the predicted normalized results shown in Fig. 13. It over-estimated model predictions at low ECR values (e.g. 5%) and under-estimated results at high ECR values. Although not very elegant, the bi-linear equation shown in Fig. 13 gives a better fit in the ECR range of interest. Generalizing this result gives:

$$(Co - Coi)/(So - Coi) = ECR/A \text{ for } ECR \leq A \quad (7)$$

$$(Co - Coi)/(So - Coi) = 1 \text{ for } ECR > A \quad (7a)$$

$$Co = Coi + (So - Coi)\,(ECR/A) \text{ for } ECR \leq A \quad (8)$$

$$Co = So \text{ for } ECR > A \quad (8a)$$

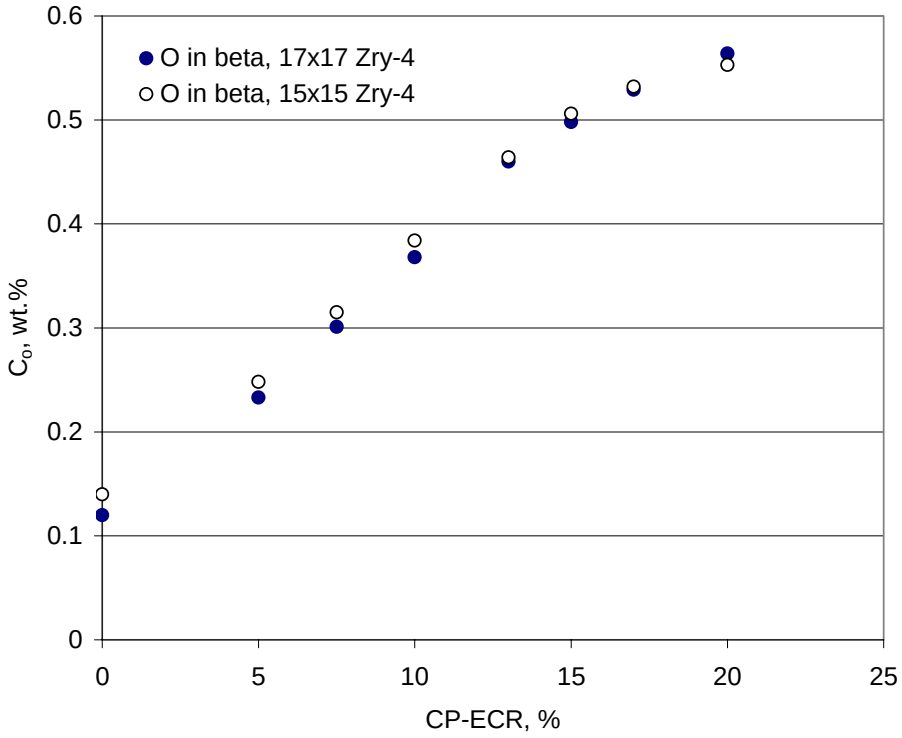

Fig. 12. Predicted average beta-layer oxygen concentration (Co) as a function of ECR for 17×17 (0.57-mm wall, 0.12-wt.% O) and 15×15 (0.76-mm wall, 0.14-wt.% O) Zry-4 cladding oxidized at 1200˚C. The oxygen solubility (So) at 1200˚C is 0.57 wt.%.

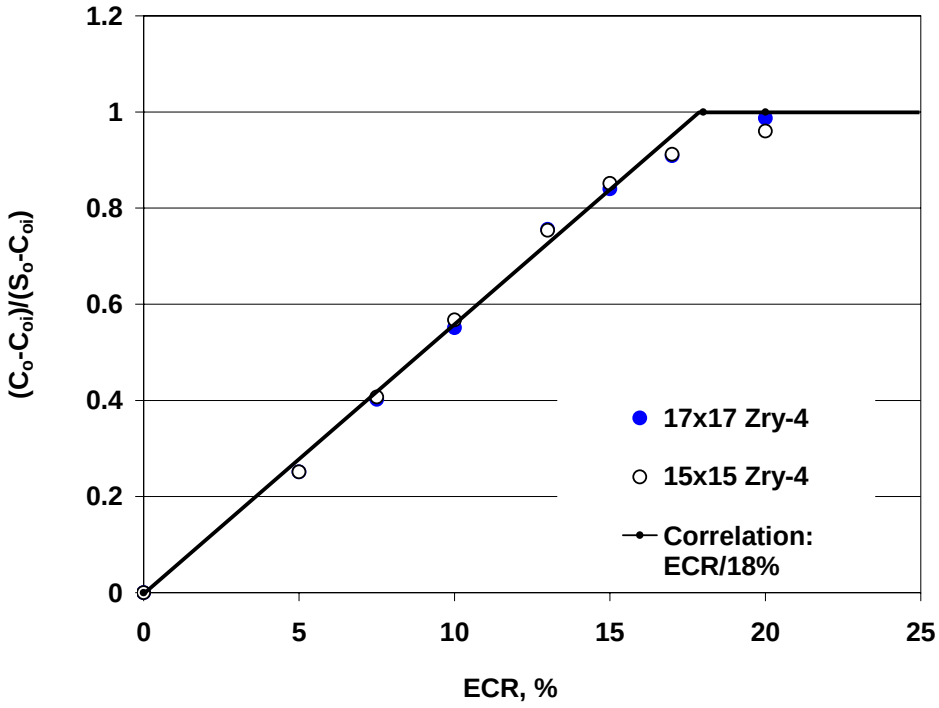

Fig. 13. Predicted normalized average beta-layer oxygen concentration as a function of ECR for 17×17 (0.57-mm wall, 0.12 wt.% O) and 15×15 (0.76-mm wall, 0.14 wt.% O) Zry-4 cladding oxidized at 1200˚C. The oxygen solubility (So) at 1200˚C is 0.57 wt.%. The straight line (ECR/18%) is a reasonable fit to the predictions for ECR ≤ 17% and is an upper-bound for predictions at > 17% ECR.

For Zry-4, oxidized at 1200˚C, the trial value for A is 18%. As the post-quench ductility data for Zry-4, ZIRLO and M5 suggest that the ductile-brittle-transition ECR for 1200˚C-oxidized samples tested at 135˚C is ≈18%, the trial value for Ccrit should be set at So = 0.57 wt.% to ensure consistency with this data set for as-fabricated cladding alloys.

Although it is anticipated that A may be a weak function of temperature and hydrogen content, it is allowed to vary with both during the data-matching phase: $A = A(T, C_h)$.

For isothermal, or near-isothermal, test conditions, A and So are constant with respect to time. The time derivative of Eq. 8 for ECR ≤ A is:

$$dCo/dt = [(So - Coi)/A]\, d(ECR)/dt \tag{9}$$

while the time derivative for ECR > A is simply zero. Integration of Eq. 9 gives:

$$Co = Coi + \int_0^F [(So - Coi)]\, d(ECR/A) \leq So \tag{10}$$

where $F = Min\{ECR_f/A, 1\}$ and ECR_f is the ECR at the end of the oxidation phase. However, Eq. 10 may not be convenient for integration because So varies with temperature and time and A may vary with temperature and time. An explicit integration with time is developed in the following.

ECR is proportional to Wg (ECR = E·Wg, where E is determined from Eqs. 1a-b) and the fundamental rate equation for Wg is

$$dWg/dt = K^2/(2\, Wg) \tag{11}$$

The expression $(E \cdot K)^2/(2\, ECR)$ can be substituted into Eq. 9 for d(ECR)/dt to derive:

$$dCo/dt = (So - Coi)\, (E \cdot K)^2/(2\, ECR/A) \tag{12}$$

Integrating Eq. 12 with respect to time, given T = T(t), gives:

$$Co = Coi + \int_0^t [(So - Coi)/A]\, (E \cdot K)^2/(2\, ECR)\, dt \leq So \tag{13}$$

For analyses of experimental data with slower heating and cooling rates, as well as for in-reactor LOCA calculations, the temperature [T(t)] dependencies of So and A would have to be included in the integration. Of the two, So would be more strongly dependent on T(t) than A would be.

5. Determination of Correlation Parameters and Correlation Validation

Using post-quench ductility data at 135˚C for as-received (ANL) and prehydrided Zry-4 (ANL and CEA), the determination of modeling parameters would proceed as follows. The CEA temperature history is closer to the isothermal case as the heating is so fast that the sample reaches 1200˚C in ≈10 s, and the sample is quenched directly from 1200˚C following the

oxidation phase. Also, the tests are one-sided so that the time at 1200˚C is very long compared to the estimated ramp time of 10 s. Post-quench ductility tests have been performed by CEA at RT on as-fabricated and prehydrided (≈300 and ≈600 wppm) Zry-4 samples oxidized at 1100˚C and 1200˚C and at 135˚C for prehydrided (≈600 wppm) Zry-4 oxidized at 1100˚C and 1200˚C [5,6,8]. From the data, the ductile-to-brittle transition ECR can be determined or at least estimated for the 600-wppm-H samples at the two oxidation temperatures. These transition ECR values (ECRcrit) are to be used in Eq. 8 along with the embrittlement oxygen concentration (Ccrit) to derive:

$$Ccrit = Coi + (So - Coi)\,[ECRcrit/A)] \tag{14}$$

The adjustable parameters are Ccrit, the parameters ΔS and a in So, and whatever dependence of A on T and C_h is needed to match the CEA data:

$$So = \exp(5.02 - 8220/T) + \Delta S\,(1 - \exp[-aC_h]) \tag{14a}$$

$$A = A(T, C_h) \tag{14b}$$

The initial values recommended for comparison are:

$Ccrit = 0.57$ wt.%

$\Delta S = 0.6$ wt.%

$a = 6\times10^{-3}$ (wppm)$^{-1}$

$A = 18\%$

If the initial values used in Eq. 14 are not consistent with the CEA post-quench ductility results, they can be adjusted such that Eq. 14 is satisfied. Given the 2 oxidation temperatures and the 1 hydrogen level leading to embrittlement within test ECR values, there are 2 ECRcrit (ductile-to-brittle transition ECR) values for use in determining parameters in Eq. 14.

Following parameter adjustment using the CEA data, the ANL two-sided 1200˚C-oxidation data (Fig. 14 for T = T(t) and Fig. 8 for post-quench ductility results) will be used. For the ANL data set, the hydrogen content is varied and the CP-ECR is held constant at 7.5% and 10%. Embrittlement occurs at ≈400 wppm for 7.5% CP-ECR and ≈300 wppm for 10% CP-ECR. The post-quench ductility data shown in Fig. 9 and the T = T(t) in Fig. 15 for prehydrided 15×15 cladding can be used to deduce ECRcrit = 5% at 600-wppm H. Because the ramp rate from 1100˚C to 1200˚C is relatively slow for both cladding types, Eq. 13 must be integrated over the T(t) histories shown in Figs. 14-15. The correlation parameters determined from the CEA data will be used in the initial calculation. These may have to be modified to match the ANL data, subject to the constraint that the set of modified values is consistent with Eq. 14 for the CEA data.

The ANL data sets for prehydrided Zry-4 give 3 critical ECR values at 3 hydrogen levels for maximum oxidation temperature of ≈1200˚C. The combined ANL and CEA data sets give 4 ductile-to-brittle transitions for determination of correlation parameters at 1200˚C.

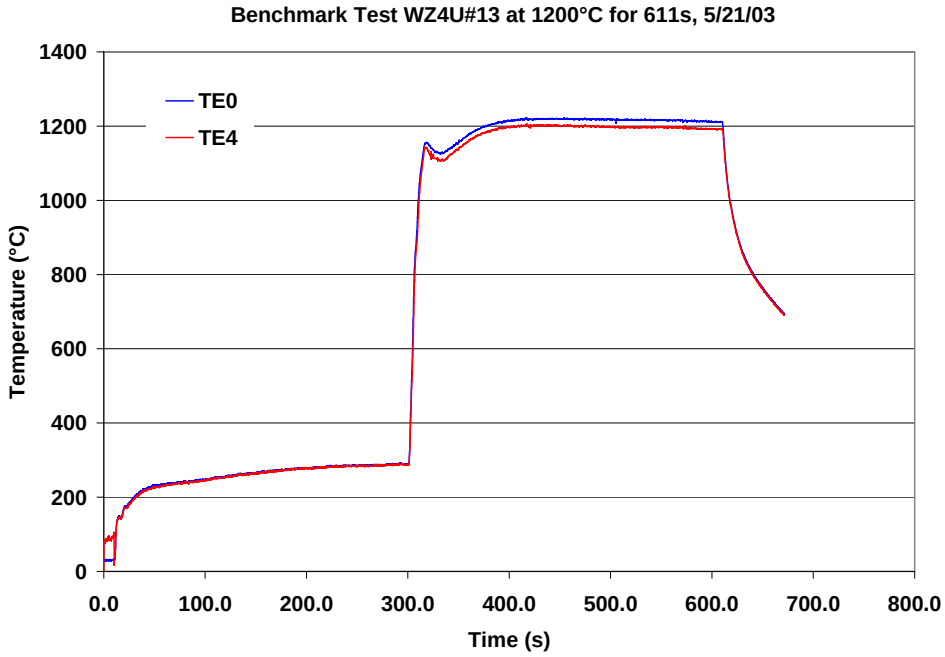

Fig. 14. Temperature history for 1200˚C-oxidation of as-received and prehydrided 17×17 Zry-4.

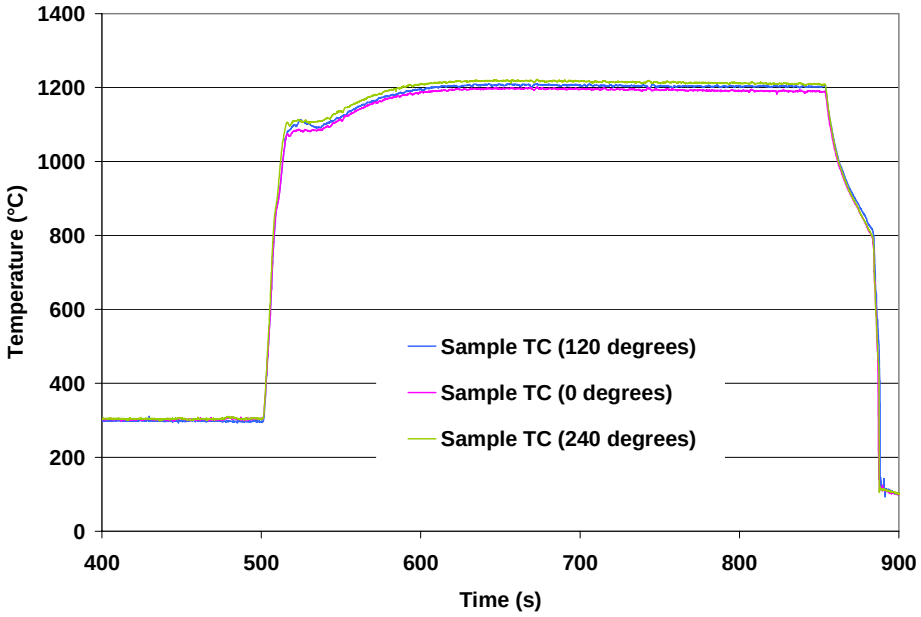

Fig. 15. Temperature history for 1200˚C-oxidation of as-received and prehydrided 15×15 Zry-4.

6. Discussion

6.1 Embrittlement of as-fabricated and prehydrided cladding

The proposed LOCA embrittlement correlation assumes a critical average oxygen concentration (Ccrit) in the prior-beta layer leading to ductile-to-brittle transition for post-quenched Zry-4 tested at 135˚C. Also proposed is a rate equation for predicting the increase in average beta-layer oxygen concentration (Co) as a function of increasing ECR, with Co saturating at the solubility limit So. Embrittlement is assumed to occur when Co = Ccrit, where Ccrit is estimated to be ≈0.57 wt.%. Under test conditions for which So < Crit, then oxygen embrittlement of the prior-beta layer cannot occur. These test conditions for as-fabricated Zry-4 include isothermal oxidation temperatures of 1000˚C (So = 0.24 wt.%) for test times ≤1.2 h, 1100˚C (So = 0.38 wt.%) and <1200˚C (So < 0.57 wt.%). ANL ring-compression test results for as-fabricated 17×17 Zry-4 support the absence of embrittlement for samples oxidized (two-sided) at these temperatures up to the highest CP-predicted ECR values used in testing program: 20% ECR at 1000˚C, 20% ECR at 1100˚C, and 17% ECR at 1200˚C. Although expressions for oxygen saturation in the beta layer have not been developed yet for ZIRLO and M5, it should be noted that these alloys demonstrate higher levels of post-quench ductility at 135˚C than Zry-4 when they are oxidized for the same time-at-temperature. The CP-ECR for ZIRLO is the same as for Zry-4, as both alloys tested have the same thickness (0.57 mm). For M5, the CP-ECR values are slightly less for the same test time because of the thicker wall (0.61 mm). Test times at 1000˚C and 1100˚C were extended for M5 samples to achieve ≈20% CP-ECR, while the CP-ECR for 1200˚C-oxidized samples tested at 135˚C was ≈16%.

Although oxygen-induced embrittlement of the prior-beta layer is not predicted for Zry-4, ZIRLO and M5 oxidized at <1200˚C, continued oxidation beyond the maximum ECR levels in the ANL program will eventually result in brittle ring-compression behavior due to the thickening of the brittle oxide and oxygen-stabilized-alpha layers and thinning of the prior-beta layer. Extended test times (>1.2 h) at 1000˚C may also lead to embrittlement due to breakaway oxidation. For 17×17 Zry-4 oxidized to 20% CP-predicted ECR, the predicted beta-layer thickness is ≈0.36 mm for oxidation temperatures of 1000-1200˚C. However, the measured beta-layer thickness for the 1200˚C sample is only 0.266 mm, indicating that CP-model predictions over-estimate beta layer thickness at high ECR values. The comparison between predicted and measured beta-layer thickness is shown in Fig. 16 for Zry-4. The measured value at 13% CP-ECR is in good agreement with the predicted value, while the measured value at 20% CP-ECR is considerably lower than predicted. Based on these two data points, the agreement between predicted and measured beta-layer thickness is good for CP-ECR ≤ 13%. Thus, rather than set a minimum value for calculated beta layer thickness, it is more practical to set a limit on CP-ECR, which agrees with measured ECR (i.e., weight gain) for Zry-4 up to the highest CP-ECR = 20% used in the ANL program. Although clearly conservative for 1100˚C Zry-4 post-quench ductility, the limit CP-ECR ≤ 18% is chosen both to protect the beta layer from excessive thinning leading to brittle ring-compression failure at 135˚C and to ensure continuity in the embrittlement predictions, especially for oxidation temperatures in the range of 1150-1204˚C. A time limit of 1 hour above 800˚C is also imposed to protect against breakaway oxidation at 800-1050˚C. The peak cladding temperature (PCT) of 1204˚C is retained as a limit in this current work.

Hydrogen causes an increase in the oxygen solubility and an increase in the oxygen pick-up rate in the beta layer. Thus, it causes embrittlement at much lower ECR values than would be observed in the 1000˚C (>20% CP-ECR), 1100˚C (>20% CP-ECR) and 1200˚C (>17% CP-ECR) oxidation-temperature tests. CEA has measured prior-beta-layer oxygen content for 1200˚C-oxidized Zry-4 samples prehydrided to ≈300 and ≈600 wppm. Similar data would be needed at oxidation temperatures of 1000˚C and 1100˚C to determine the possible temperature dependence of the parameter "a" in the solubility expression (Eq. 4). In the absence of such data, the temperature dependence of "a" at 1000˚C and 1100˚C can be determined indirectly by matching post-quench ductility data at these oxidation temperatures. It should also be emphasized that the effects of hydrogen on oxygen solubility may be alloy dependent.

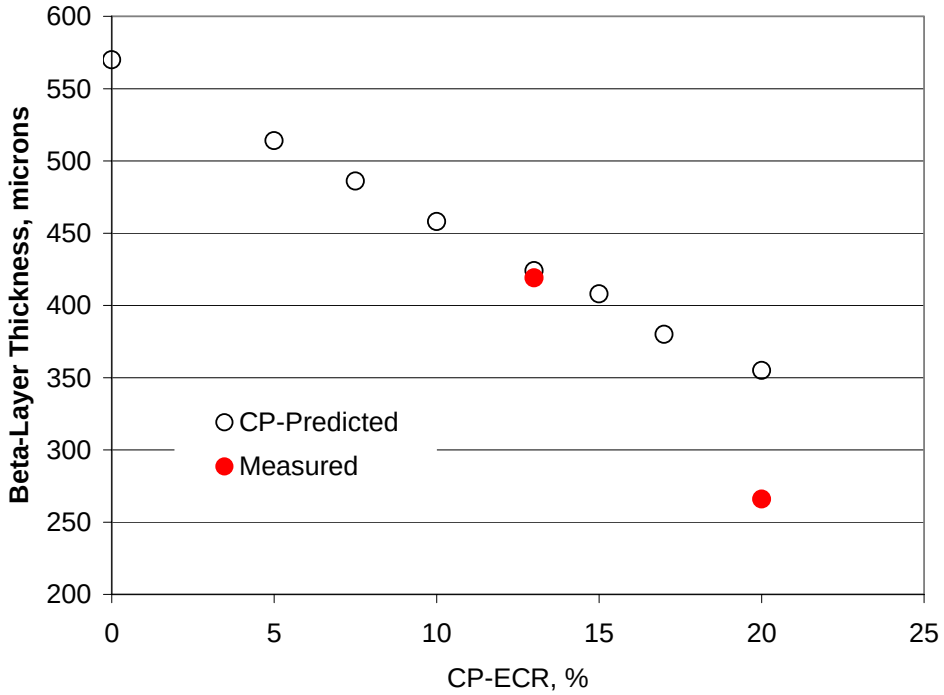

Fig. 16. Cathcart-Pawel predicted vs. measured values of the prior-beta layer thickness following two-sided steam oxidation of 17×17 Zry-4 (0.57-mm wall) at 1200˚C.

6.2 Embrittlement of Irradiated Cladding

The steam-oxidation behavior of irradiated cladding with a waterside corrosion layer and a fuel-side bond layer is not well characterized, particularly for the low test times of interest. Most studies (e.g., ANL Zry-2, IRSN Zry-4, JAERI Zry-4) have been conducted at high test times and high predicted ECR values. The results of these studies generally suggest that the corrosion layer is not protective and that corroded cladding oxidizes at about the same rate as bare cladding. However, early time oxidation behavior of irradiated cladding cannot be discerned from these high ECR tests. For example, a test time corresponding to 20% predicted ECR may lead to 18% measured ECR. As the measured ECR is within 10% of the predicted ECR, then the conclusion that the corrosion layer is not protective seems reasonable. For double-sided oxidation tests using irradiated cladding, it would be useful to see a direct comparison between the outer- and inner- oxide layer thickness values. If the outer-surface oxide layer is thinner, then the results would suggest partial protection of the coolant-side corrosion layer.

Recently, ANL conducted a series of two-sided oxidation tests at ≈1200˚C with high-burnup Zr-4 cladding. The temperature history, based on thermal benchmark tests with as-fabricated (i.e., bare) cladding, is shown in Fig. 17, along with the CP-predicted ECR values for each test. The high-burnup Zry-4 samples oxidized to CP-ECR values of 3, 5, 7, 8 and 10% had a corrosion layer of ≈70 μm, a fuel-cladding bond layer of ≈10 microns and a hydrogen content of 550±90 wppm. These samples were cooled at ≈10˚C/s from their maximum oxidation temperature to 800˚C, slow-cooled to RT and ring-compressed at 135˚C. One sample with a 95-μm corrosion layer and 800±110 wppm hydrogen oxidized to CP-ECR = 8% was quenched from 800˚C to 100˚C and slow cooled to room temperature. The surprisingly high post-quench ductility of the 3 and 5% CP-ECR samples and the low-but-not-zero ductility of the 7 and 8% CP-ECR samples (see Fig. 18) suggest that the weight gain, oxygen content in the prior-beta layer and corresponding ECR were all less than predicted. The results also suggest that the corrosion layer is a source of oxygen for diffusion into the cladding, as well as being partially protective.

Detailed metallographic examination was performed on the 8% CP-ECR sample. Figure 19 shows an optical microscopy image near the outer surface of one of 8 locations examined. There are three oxide zones observed at the cladding outer surface: oxide layer from corrosion layer, from transition layer and from steam-induced oxide layer. The weight gain and "measured" ECR were calculated by including most of the transition layer in the calculation. Based on quantitative analysis, the average steam-oxide layer near the cladding outer- and inner-surfaces was calculated to be 20 μm and 26 μm, respectively. The ECR value corresponding to the weight gain is 5.8%, which is lower than the 8% CP-ECR value. However, as shown in the SEM image (Fig. 20) of a region near the one used for optical microscopy, the transition region is really a part of the corrosion layer and should not be used to calculate transient ECR due to steam oxidation. Until a new value of ECR is calculated based on what has been learned from SEM imaging, we will assume that the measured ECR for the 8% CP-ECR sample is 5.5%. Although the 10% CP-ECR sample has not been examined in detail to determine measured ECR, we will assume that the effects of the corrosion layer is a delay of 2.5% ECR, relative to the CP value. That gives us 3 data points to compare with the data for prehydrided Zry-4: 5.5% measured ECR with ≈550 wppm H, 5.5% measured ECR with ≈800 wppm H (quenched at 800˚C), and 7.5% measured ECR with about 550 wppm H. The corresponding offset strains for

these three rings are: 3.8% (ductile), 0% (brittle), and 0.5% (brittle). As shown in Fig. 21, the offset strain for the high-burnup Zry-4 samples is consistent with what was measured for prehydrided Zry-4 if the comparison is made based on measured ECR rather than CP-ECR. More data are needed to develop an embrittlement correlation based on calculated ECR for irradiated cladding with a coolant-side corrosion layer.

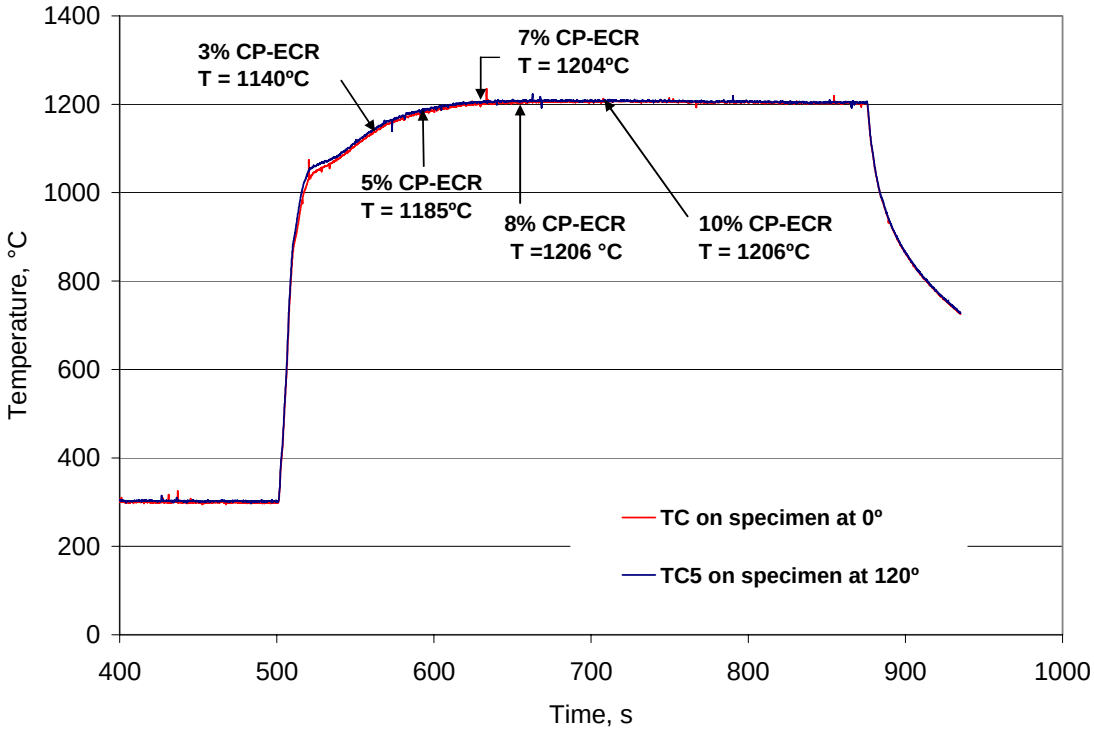

Fig. 17. Thermal response of as-fabricated 15×15 Zry-4 sample outer surface during steam oxidation in the test train used for in-cell tests. Thickness of the sample was 0.77 mm. Irradiated Zry-4 had a metal thickness of 0.71 mm and a corrosion layer of about 70 μm. The CP-ECR values shown in the figure are based on the 0.71-mm wall thickness.

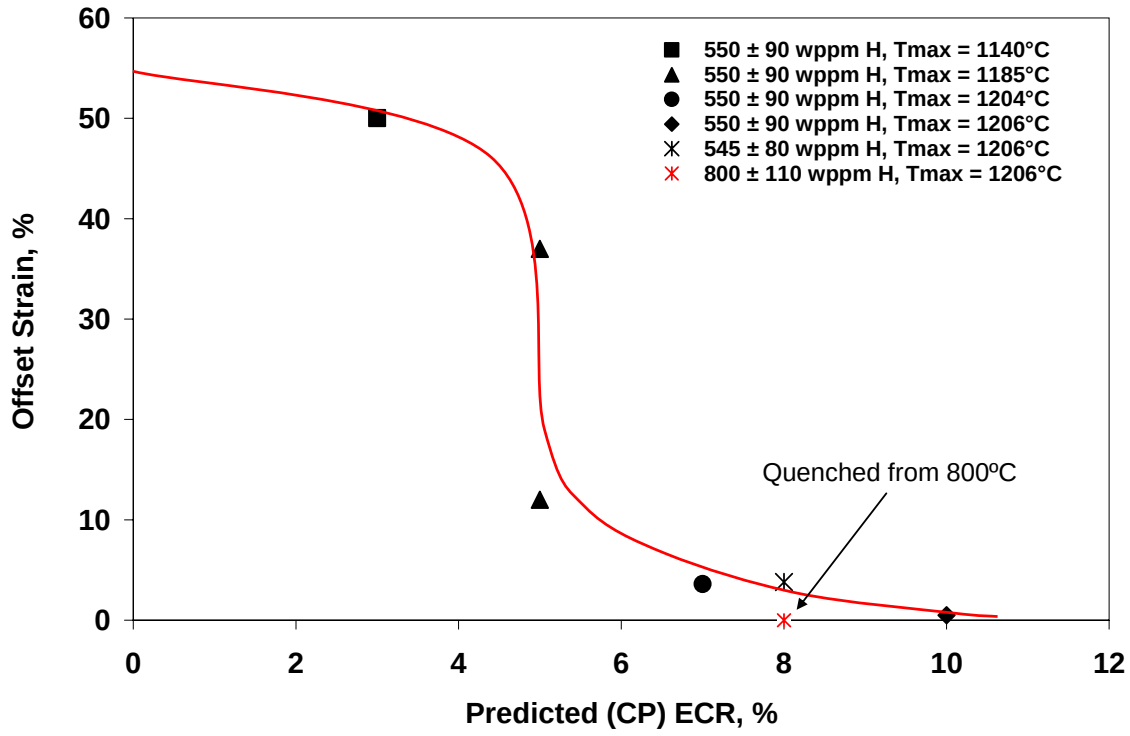

Fig. 18. Ring-compression ductility (offset strain) vs. CP-predicted ECR for the high-burnup Zry-4 cladding samples exposed to two-sided steam oxidation at times, temperatures and CP-ECR values shown in Fig. 17.

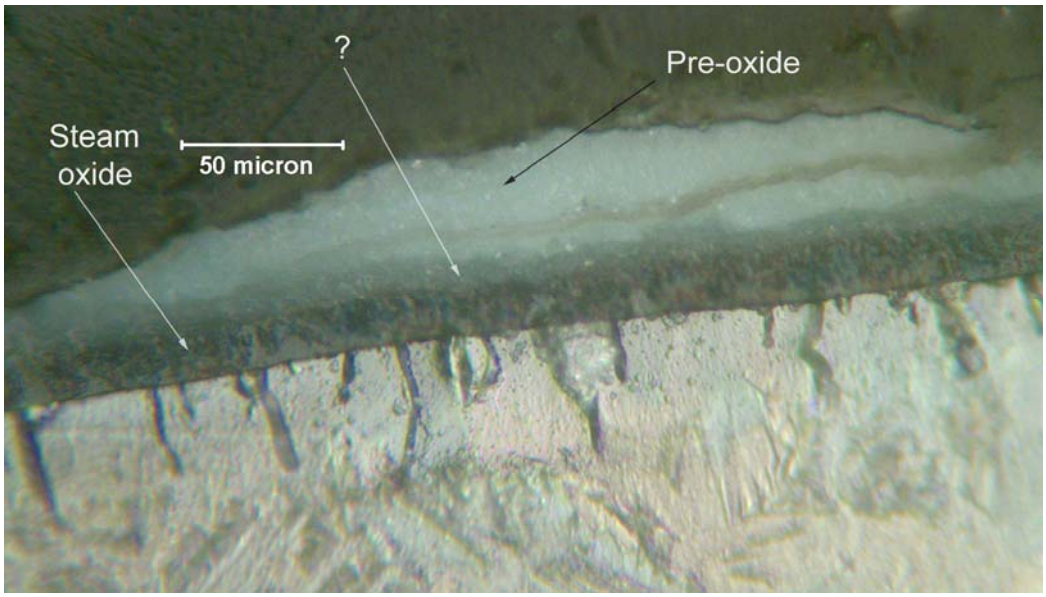

Fig. 19. Optical microscopy image of the outer surface steam-oxide and corrosion layers at one location of the high-burnup Zry-4 sample oxidized at ≈1204˚C to 8% CP-ECR. The transition region (?) was counted as part of the steam-oxide layer in the weight gain and measured ECR determination to give 5.8% measured ECR.

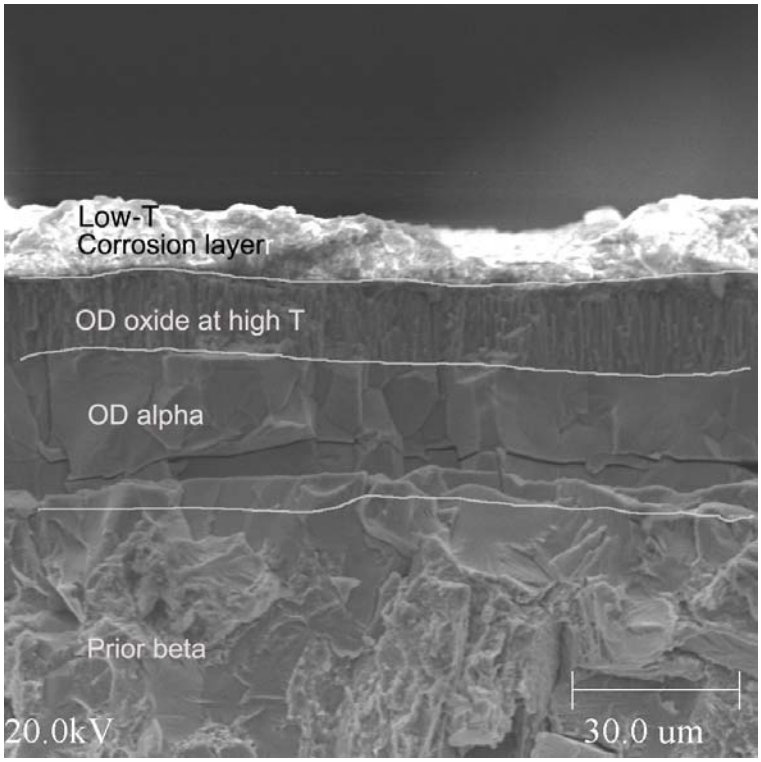

Fig. 20. SEM image showing clearer distinction between corrosion layer and steam-oxide layer (columnar morphology) at a location near the one imaged in Fig. 19 by optical microscopy.

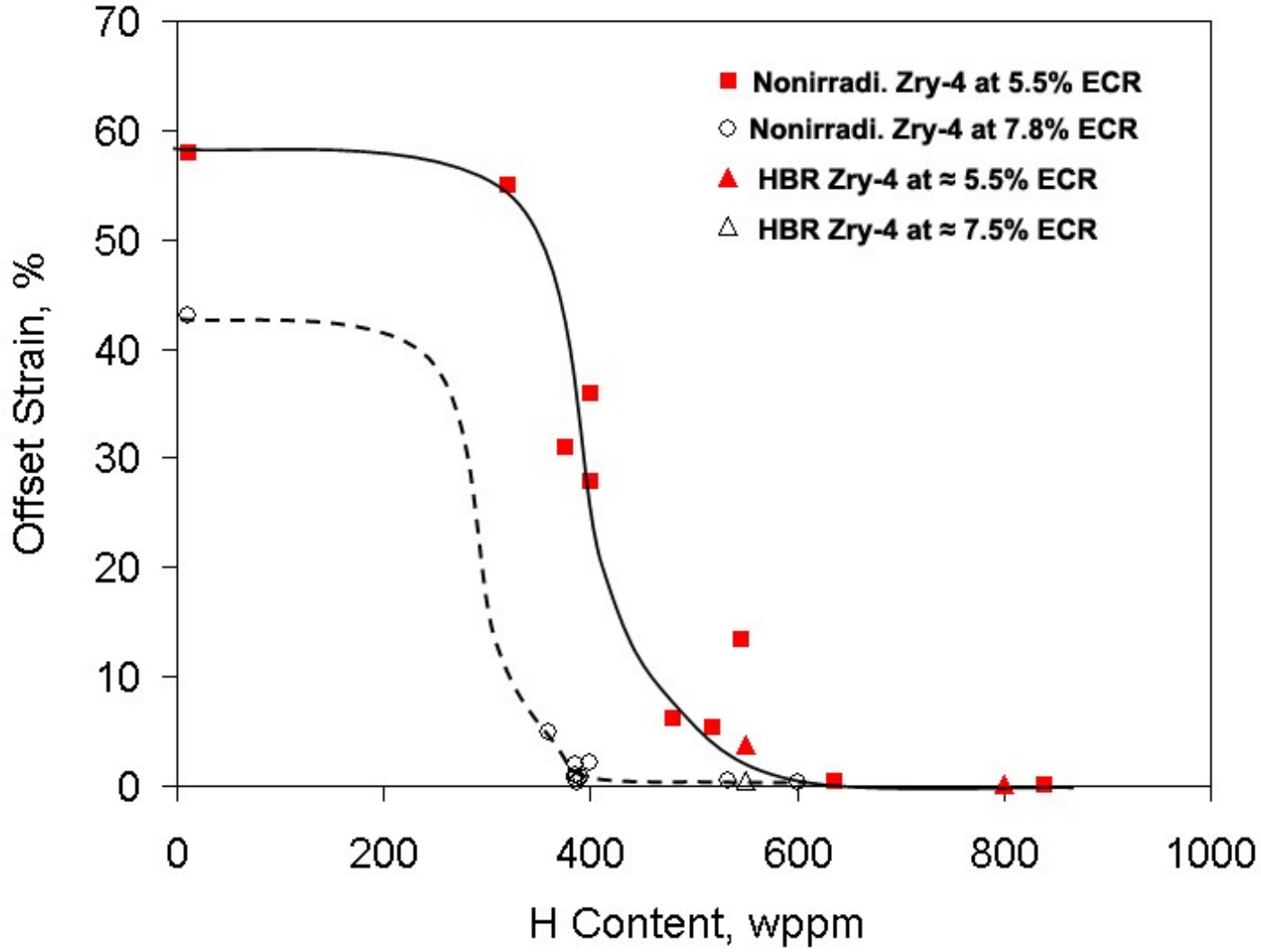

Fig. 21. Comparison of post-quench and post-oxidation ductility of prehydrided 15×15 Zry-4 and high-burnup 15×15 Zr-4 vs. hydrogen content and ECR based on measured weight gain.

References

1. D. O. Hobson, "Ductile-Brittle Behavior of Zircaloy Fuel Cladding," Proc. ANS Topical Mtg. on Water Reactor Safety, Salt Lake City, March 26, 1973, pp. 274-288.

2. H. M. Chung and T. F. Kassner, "Embrittlement Criteria for Zircaloy Fuel Cladding Applicable to Accident Situations in Light-Water Reactors: Summary Report," NUREG/CR-1344, ANL-79-48, January 1980.

3. J. V. Cathcart, R. E. Pawel, R. A. McKee, R. E. Druscel, G. J. Yurek, J. J. Cambell and S. H. Jury, "Zirconium Metal-Water Oxidation Kinetics IV. Reaction Rate Studies", ORNL/NUREG-17, Aug. 1977.

4. H. M. Chung and T. F. Kassner, "Psuedobinary Zircaloy-Oxygen Phase Diagram," J. Nucl. Mater. 84 (1979) 327-339.

5. L. Portier, T. Bredel, J. C. Brachet, V. Maillot, J. P. Mardon, and A. Lesbos, "Influence of Long Service Exposures on the Thermal-Mechanical Behavior of Zry-4 and M5^{TM} Alloys in LOCA Conditions," presented at the 14th International Symposium on Zirconium in the Nuclear Industry, Stockholm, Sweden, June 13-17, 2004, to be published in meeting proceedings.

6. J-C. Brachet, L. Portier, V. Maillot, T. Forgeson, J. P. Mardon, and A. Lesbos, Overview of the CEA Data on the Influence of Hydrogen on the Metallurgical and Thermal-Mechanical Behavior of Zircaloy-4 and M5TM Alloys under LOCA Conditions," presented at the NRC Nuclear Safety Research Conference, Washington DC, Oct. 25-25, 2004, to be published in the proceedings.

7. R. E. Pawel, R. A. Perkins, R. A. McFee, J. Cathcart, G. J. Yurek, and R. E. Druschel, "Diffusion of Oxygen in Beta-Zirconium and the High-Temperature Zircaloy-Steam Raecation," Zirconium in the Nuclear Industry, ASTM STP 633, ASTM, 1977, pp. 119-133.

8. J. P. Mardon, J. C. Brachet, L. Portier, V. Maillot, T. Forgeron, A. Lesbos and N. Waeckel., "Influence of Hydrogen Simulating Burn-up Effects on the Metallurgical and Thermal-Mechanical Behavior of M5^{TM} and Zircaloy-4 Alloys," to be presented at the 13th International Conference on Nuclear Engineering (ICONE-13), Beijing, China, May 16-20, 2005.